

A STUDY ON VIBRATION SENSORS WITH APPLICATION IN  
STRUCTURAL HEALTH MONITORING (SHM)

NAVID HAKIMITOROGHI

A THESIS  
IN  
THE DEPARTMENT  
OF  
ELECTRICAL AND COMPUTER ENGINEERING

PRESENTED IN PARTIAL FULFILLMENT OF THE REQUIREMENTS  
FOR THE DEGREE OF MASTER OF APPLIED SCIENCE  
CONCORDIA UNIVERSITY  
MONTRÉAL, QUÉBEC, CANADA

SEPTEMBER 2018  
© NAVID HAKIMITOROGHI, 2018

CONCORDIA UNIVERSITY  
School of Graduate Studies

This is to certify that the thesis prepared

By: **Navid Hakimitoroghi**  
Entitled: **A study on vibration sensors with application in structural health monitoring (SHM)**

and submitted in partial fulfillment of the requirements for the degree of

**Master of Applied Science**

complies with the regulations of this University and meets the accepted standards with respect to originality and quality.

Signed by the final examining committee:

Dr. D. Qiu \_\_\_\_\_ Chair  
Dr. A. Awasthi \_\_\_\_\_ External Examiner  
Dr. G. Cowan \_\_\_\_\_ Internal Examiner  
Dr. R. Raut \_\_\_\_\_ Supervisor  
Dr. A. Bagchi \_\_\_\_\_ Co-Supervisor

Approved \_\_\_\_\_  
Chair of Department or Graduate Program Director

\_\_\_\_\_ 20 \_\_\_\_\_

Rama Bhat, Ph.D.,ing., FEIC, FCSME, FASME, Interim Dean  
Faculty of Engineering and Computer Science

# Abstract

A study on vibration sensors with application in structural health monitoring (SHM)

Navid Hakimitoroghi

With the prolific usage of vibration analysis to extract information about different structures (buildings and bridges etc.), vibration sensors have become an important device in Structural Health Monitoring (SHM). In this study, we tried to modify the previous generation of vibration sensors in the analog front end and build a new prototype for a vibration sensor with applications in SHM.

A vibration sensor system includes different modules. Each module has its own functionality. In a vibration sensor system, all these modules have to work together deliberately to form a sensor system. Among the modules that form a sensor system, analog sub-system is responsible to prepare the output signal of the seismic sensor for the analog-digital converter. Mass-spring velocity meter (geophone) which is one of the mostly used sensor in SHM is the main seismic sensor in our sensor prototype. In each geophone, vibrations below a certain frequency which is called corner frequency, is hard to detect because of geophone frequency response. Several techniques have been proposed in this study to modify the lower frequency response of the geophone.

We have verified the compensation techniques in two different situations. First, using a shake table, we excited the geophone with different frequencies and evaluated the compensated frequency response. For the final verification in a real test environment, we tested qualification of the geophone in detecting the vibration of a real building at low frequencies.

# Acknowledgments

First and foremost I offer my sincerest gratitudes to my supervisors, Dr. Rabin Raut and Dr. Ashutosh Bagchi, who have supported me throughout my thesis with their patience and knowledge whilst allowing me room to work in my own way. I attribute the level of my Masters degree to their encouragement and effort and without them this thesis, too, would not have been completed or written. One simply could not wish for better or friendlier supervisors.

I also have to mention my parents for their inseparable support and prayers.

I also acknowledge the support of the Natural Sciences and Engineering Research Council of Canada (NSERC) and Sensequake<sup>TM</sup> for this study.

Finally, I would like to thank everybody who was important to the successful realization of the thesis, as well as expressing my apology that I could not mention personally one by one.

# Contents

<b>List of Figures</b>	<b>vii</b>
<b>List of Tables</b>	<b>ix</b>
<b>1 Introduction</b>	<b>1</b>
1.1 Seismic Sensor System . . . . .	2
1.1.1 Seismic Sensor . . . . .	3
1.1.2 Other Modules of a Sensor System . . . . .	3
1.2 Problem Statement . . . . .	5
1.3 Literature Review . . . . .	6
1.4 Thesis Overview . . . . .	8
<b>2 Seismic Sensors</b>	<b>10</b>
2.1 Geophone (velocity meter) . . . . .	10
2.2 MEMS Accelerometers . . . . .	12
2.3 Piezoelectric Accelerometers . . . . .	13
2.4 Some important functional parameters of vibration sensors . . . . .	14
2.4.1 Sensitivity . . . . .	14
2.4.2 Dynamic Range . . . . .	15
2.4.3 Linearity . . . . .	15
2.4.4 Gain . . . . .	15
2.5 Sensor Selection for the Sensor System . . . . .	15
2.6 Chapter Summary . . . . .	16
<b>3 Example of a Modern Sensor System</b>	<b>17</b>
3.1 Vibrations recording . . . . .	18
3.2 Synchronization . . . . .	19
3.3 Wireless communication for data transfer . . . . .	22
3.4 Chapter Summary . . . . .	24
<b>4 Analog Subsystem</b>	<b>25</b>
4.1 Amplifiers . . . . .	25

4.2	Filter . . . . .	27
4.3	Frequency Response Compensator . . . . .	27
4.3.1	Passive Response Compensator . . . . .	29
4.3.2	Inverse Transfer Function Response Compensator . . . . .	30
4.3.3	Multi-Loop Feedback Method for Compensation . . . . .	32
4.3.4	Modified Multi-Loop Feedback Method for Compensation . . . . .	34
4.4	Chapter Summary . . . . .	36
<b>5</b>	<b>Experimental Results</b>	<b>37</b>
5.1	Test Plans . . . . .	37
5.1.1	Test Plan 1 . . . . .	37
5.1.2	Test Plan 2 . . . . .	37
5.1.3	Test Plan 3 . . . . .	38
5.1.4	Test Plan 4 . . . . .	39
5.2	Equipment and Setup . . . . .	40
5.3	Measurements . . . . .	43
5.3.1	Measurements for Test Plan 1 . . . . .	43
5.3.2	Measurements for Test Plan 2 . . . . .	44
5.3.3	Measurements for Test Plan 3 . . . . .	45
5.3.4	Measurements for Test Plan 4 . . . . .	47
5.4	Chapter Summary . . . . .	49
<b>6</b>	<b>Buiding Test</b>	<b>50</b>
6.1	Test Plan . . . . .	50
6.2	Measurements . . . . .	51
6.3	Discussion of the Test Results . . . . .	56
<b>7</b>	<b>Conclusions and Future Works</b>	<b>57</b>
7.1	Conclusions . . . . .	57
7.2	Future Works . . . . .	57
7.2.1	Analog Subsystem . . . . .	58
7.2.2	At The Sensor Level . . . . .	58

# List of Figures

1	Basic mass-spring seismometer . . . . .	1
2	a) A sample building; b) to e) layout of sensors array (from <a href="http://www.sensequake.com">www.sensequake.com</a> ) . . . . .	2
3	Visualized model of the building (from <a href="http://www.sensequake.com">www.sensequake.com</a> ) . . . . .	3
4	System overview of a sensor prototype . . . . .	4
5	Overview of the wireless network for an array of sensors . . . . .	5
6	Geophone structure . . . . .	10
7	Frequency response of GS11-D for two different loads [1] . . . . .	11
8	Housing for a three axis sensor system (photo from: <a href="http://www.sydneystormcity.com">www.sydneystormcity.com</a> ) . . . . .	12
9	MEMS accelerometer internal structure . . . . .	12
10	Piezoelectric accelerometer internal structure [2] . . . . .	14
11	NUCLEO-L476RG Evaluation board of the MCU . . . . .	18
12	Modules that are engaged in the vibration recording . . . . .	19
13	Modules that are engaged in the synchronization . . . . .	20
14	DUST network kit for sensor evaluation . . . . .	20
15	DUST module to mount on the prototype board . . . . .	21
16	U-blox NEO-M8Q-01A GPS module [3] . . . . .	21
17	Modules that are engaged in the data transfer . . . . .	22
18	SPWF04SA expansion board for the Wi-Fi . . . . .	23
19	Sensor system overview . . . . .	23
20	(a) analog subsystem for the geophone (b) analog subsystem for the analog MEMS . . . . .	25
21	Instrumentation amplifier [4] . . . . .	26
22	Non-inverting amplifier . . . . .	27
23	Passive RC filter for differential ADC . . . . .	27
24	Geophone model with separated components for the coil [5] . . . . .	28
25	Geophone equivalent circuit with current source . . . . .	29
26	Geophone equivalent circuit simulation result. Magnitude (solid blue line) and phase (dashed blue line) . . . . .	29
27	Passive compensator structure . . . . .	30
28	Passive compensator circuit . . . . .	30
29	Passive compensator numerical simulation result . . . . .	31
30	Circuit for inverse transfer function technique . . . . .	31

31	Inverse transfer function compensator circuit simulation . . . . .	32
32	Geophone cascaded with an unknown impedance $Z(s)$ . . . . .	32
33	Realization of the admittance $Y(s)$ using lossless integrators . . . . .	33
34	Schematic of $T(s)$ analogue of $Y(s)$ in Eq. 9 . . . . .	34
35	Admittance converter . . . . .	34
36	Circuit simulation result of the multi-loop feedback method for compensation . . . . .	35
37	Realization of the admittance $Y(s)$ using lossy integrators . . . . .	35
38	Schematic of voltage transfer function analogue of $Y(s)$ in Eq. 11 using lossy integrators	36
39	(a) Test setup; (b) Analog subsystem for case 1; (c) Analog subsystem for case 2 . . .	38
40	Piezoelectric sensor . . . . .	39
41	(a) Test setup for the piezoelectric sensor; (b) Test setup for the geophone; (c) Analog subsystem for the geophone (c) . . . . .	39
42	The lab equipments for the experiments . . . . .	40
43	The Shaker structure . . . . .	41
44	DC222A-B: ADC evaluation board (left). DC890B: PC interface board (right) . . .	42
45	Screenshot of the Pscope software for a test . . . . .	42
46	Geophone frequency response. Simulation vs. result of experiment . . . . .	43
47	Compensated geophone Vs. geophone. Shaker at 0.1 $Hz$ . . . . .	44
48	Compensated geophone Vs. geophone. Shaker at 1 $Hz$ . . . . .	44
49	Impedance for the multi-loop feedback technique for geophone response compensator. Simulations vs. result of experiment . . . . .	45
50	Compensated geophone vs. piezoelectric sensor response in low frequencies . . . . .	46
51	Filtering effect of multi-loop feedback method vs inverse transfer function method . .	46
52	Compensated geophone vs. piezoelectric sensor response in low frequencies . . . . .	48
53	Filtering effect of modified multi-loop feedback method vs inverse transfer function method . . . . .	48
54	EV building, Concordia University (from <a href="http://www.concordia.ca">www.concordia.ca</a> ) . . . . .	50
55	The plan of 16th floor of EV building . . . . .	51
56	EV building vibration test in spot 1 (See Fig. 55) . . . . .	52
57	EV building vibration test in spot 2 (See Fig. 55) . . . . .	53
58	EV building vibration test in spot 3 (See Fig. 55) . . . . .	54
59	EV building vibration test in spot 4 (See Fig. 55) . . . . .	55
60	EV building vibration test in spot 5 (See Fig. 55) . . . . .	56

# List of Tables

1    Vibration related parameters in different situations [6] . . . . . 15

# Chapter 1

## Introduction

The advances in seismology started with the availability of precise seismometer from 1900 and afterwards. Using primary seismometers, the scientists could measure the magnitude of earthquakes. Using seismometers scattered in a large area with more accurate timing, they could locate the position of the earthquake by the evaluation of the delays in earthquake vibrations. At this point, the seismometers were not sensitive enough to measure smaller vibrations. For more precise applications in geological sciences (i.e., evaluation of the natural movement of the earth's crust) one needed to have information about the natural background vibrations. With this demand on detecting and processing of vibrations of the earth, knowledge on vibration sensors, and applying these for processing vibration signals have become vital in geology and seismology.

Beside the magnitude of a vibration, the rate of changes in the vibration with time has a vital role in seismic investigations. This item is defined as the frequency of the vibration. The frequency band of the vibrations in seismology ranges from  $0.1 \text{ Hz}$  to  $1000 \text{ Hz}$ . The range of frequencies for different events is shown Tab. 1.

It is practically impossible to design one sensor to cover the wide range of magnitudes and frequencies. Therefore, sensor designers focus on building sensors that meet the requirements for a specific application. [7].

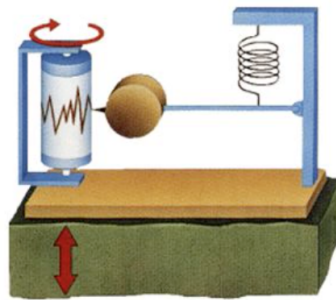


Figure 1: Basic mass-spring seismometer

One of the specific applications of the vibration sensors is in structural and civil engineering. Civil engineers could extract important information about the structure by analyzing the vibration profile of the structure. Extracted information is useful to model and predict the structural behavior in earthquakes. This model is used to predict the behavior of the structure during an earthquake. Therefore, based on the perditions, they can reinforce the structure to prevent disastrous collapse in case of severe earthquakes.

Evaluation of the seismic performance of a structure is also possible using numerical methods. These numerical methods are based on linear or non-linear dynamic analysis and have different results due to using different approaches employed to reach the result. On the other hand, the data used for such method is mainly gathered from the technical drawings of the building which are not accurate enough (especially for older buildings) [8].

One of the investigation methods that is extensively explained in [8] is ambient vibration testing (AVT). This method utilizes ambient vibrations that have been gathered by an array of sensors to predict the seismic performance of the buildings. Fig. 2 shows a building under test with four different constellations of sensors (red spot) to measure the vibrations. Location of each sensor is predefined by the structural specialists. The target of this study is to develop an improved sensor

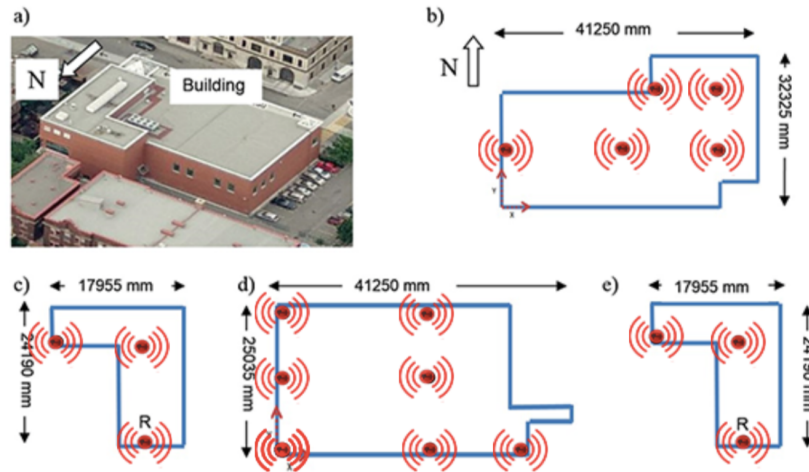


Figure 2: a) A sample building; b) to e) layout of sensors array (from [www.sensequake.com](http://www.sensequake.com))

device which could fit the applications that approaches the seismic performance evaluation similar to AVT.

The seismic sensor system, its components and structure are briefly explained in the following sections.

## 1.1 Seismic Sensor System

A seismic sensor system is an instrument to measure and record the vibration of the ground or any other moving structure. Regarding the application, the sensor may be used as a single unit (i.e.

bearing vibration sensor) or as an array of sensors (i.e. seismic evaluation sensor in SHM). In case of using an array of sensors, they must be equipped with adequate facilities to manage the time synchronization among the sensors, communication of each sensor with a host, data storage, etc. Later, the gathered data from all the sensors can be processed in a software for more interpretation by the structural engineering specialists. Fig. 3 shows one the results of analyzing the building that is showed in Fig. 2. Note that in the visualization, the vibrations are always exaggerated to have more visibility.

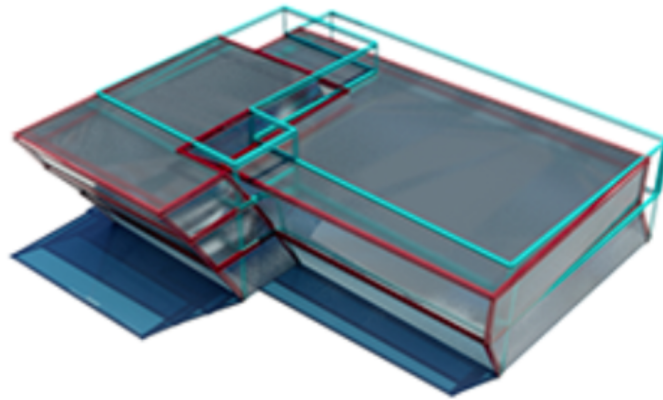


Figure 3: Visualized model of the building (from [www.sensequake.com](http://www.sensequake.com))

### 1.1.1 Seismic Sensor

The main component of each seismic sensor system is a seismic sensor. A seismic sensor generates a physical signal (i.e. voltage or current) regarding the motions of the body of the sensor. Seismic sensors, traditionally work based on a mass - spring structure (Fig. 1).

All the information about the deifferent type of seismic sensors that have been used in this study is discussed in the next chapter.

### 1.1.2 Other Modules of a Sensor System

As mentioned before, besides the sensors, other modules and components have to be added to form the seismic sensor system. Fig. 4 shows a system diagram containing the modules that can be used in a prototype sensor system. Among all the module that have been shown if Fig. 4, some of them (i.e. GPS) are not mandatory for a sensor system.

The functions of the different modules which are necessary for a sensor system are briefly discussed below.

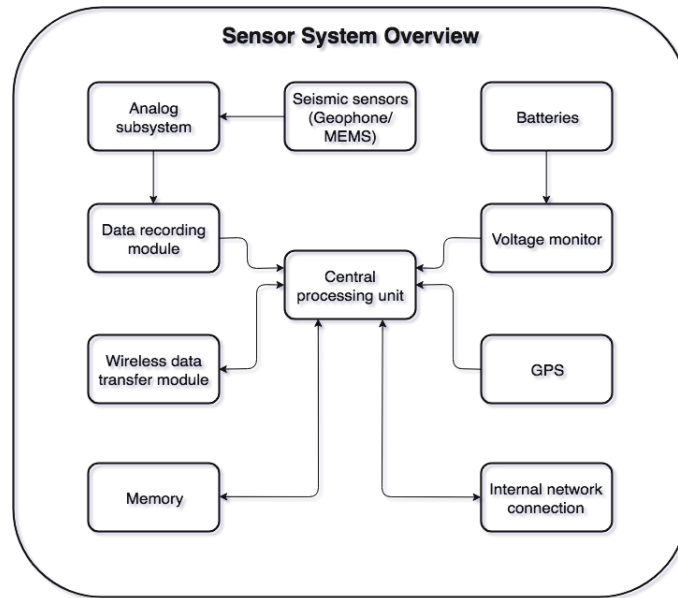


Figure 4: System overview of a sensor prototype

### Analog subsystem

A seismic sensor system may contain one or more vibration sensors. In case of utilizing geophones, a compensator is required to reconstruct very low-frequency vibration signals. An amplifier, a gain control circuit, and an anti-aliasing filter is required to introduce a clean signal to the analog-digital converter (ADC). Functions of these modules have been adequately explained in the following chapters. In case of using analog MEMS accelerometers, all the circuits except the compensator are required. Note that the impedance matching, especially for the first stage of analog circuitry, plays a vital role to deliver a clear signal to the data recording module.

### Data recording module

The data recording module which follows the analog subsystem, can be a standalone ADC or an internal ADC of a microcontroller. This module is responsible to sample the data at a fixed interval and deliver the sample to the MCU (microcontroller). As the interface between the analog front end modules and the digital data, it is necessary to choose an optimum ADC with low level of noise and high resolution to record the data.

### Wireless module

At least one internal network connection is required to synchronize the sensors array. In this network, a pilot signal broadcasts from the host sensor to keep the track start command, stop command and synchronization of the internal clock of each sensor.

A second optional wireless connection is also used in some commercial sensors that connect a remote device for the different usage (trigger the start and stop command for the test or gathering the data

after the test). Fig. 5 shows a typical wireless network for a seismic sensor system. In this figure, one of the sensors (hub sensor) can communicate with the remote device over a Wi-Fi connection. The rest of sensors (inside the cloud) are connected together in another network.

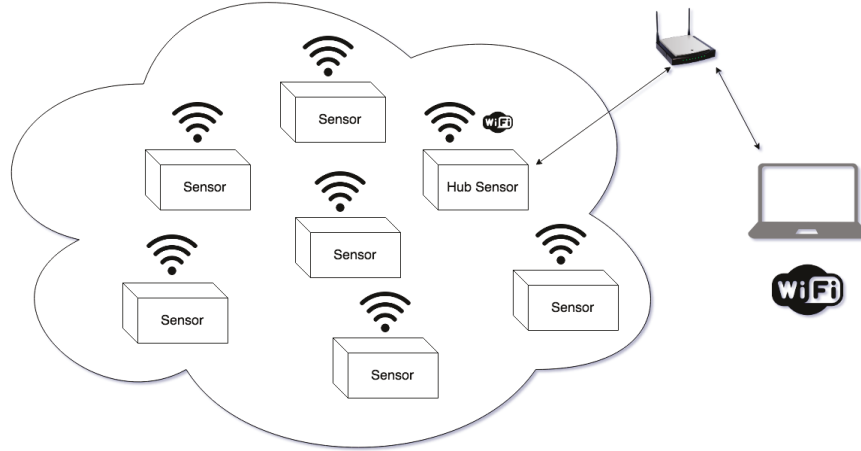


Figure 5: Overview of the wireless network for an array of sensors

### Data storage module

This unit saves the recorded data of the tests for later analysis. As mentioned, in some sensors, the data can be transmitted to the host after the test. In these cases, the storage is considered as a backup option to prevent data loss due to failure in wireless connection.

## 1.2 Problem Statement

In this study, we targeted to improve some of the weaknesses of the available commercial sensors as far as the low frequency response is concerned. Although the proposed circuit in this work is matched with GS11-D geophone, by small changes in the design parameters, they can be used for other geophones. As mentioned before, response of a geophone to vibrations below the corner frequency is attenuated due to the internal mechanical structure of the device. So, in this work we targeted to design an analog circuitry for the sensor system which could reduce or eliminate this impairment at low-frequencies response. Circuit and numerical simulations results (LTSPICE and MATLAB) are verified by experimental tests.

To measure the vibrations, this analog circuit have to operate in a sensor system. Design of the sensor system is the next target of this study.

## 1.3 Literature Review

In this section, we want to review the related researches, works and products that have been done before this research work.

In the sensor level, we had worked with Tromino [9] as a product and studied [10] as a patent for a sensor system design.

[10] is a patent that introduces a sensitive sensor system for application in SHM. Regarding the specifications that are defined in SHM, this sensor system has a seismic sensor, a low-pass filter, a gain amplifier, an ADC and a wireless module that connects the sensors in different locations. The only seismic sensor that has been used in this sensor system is an accelerometer. Geophones are often more sensitive compared to the accelerometers. Therefore, it is preferable to use geophone for sensor system with applications in SHM.

Tromino is a commercial sensor that has been used for SHM application. Tromino has three geophones to measure the vibration in three directions. Besides geophones, it has a MEMS accelerometer with lower sensitivity compared to geophone. Two signal paths from the geophone with two different gains are considered in the analog subsystem without compensation on low frequency response of the geophone. The weaknesses that we tried to address in our sensor prototype are improvements on analog subsystem and improvements on wireless connection. For the analog subsystem, regarding the low frequency response of the geophone, it is necessary to have the response compensator. For the wireless connection, different sensors in an array of Tromino sensors only can record the data in their internal storage. Therefore, after each test, the user have to download the data for consequent tests from each sensor individually by cable connected to a PC.

We investigated other possible improvements on the Tromino. These possible improvements are on the resolution and noise level of the ADC, internal and external wireless network that synchronizes the sensors, power management and updatability of the sensor system. The above mentioned improvements and their related literatures are presented in chapter 3. In the following we reviewed the literatures related to the low frequency response compensation of the geophone.

In order to compensate the geophone response in low frequencies, the researchers generally used three different approaches:

- Compensation by modifying the geophone structure
- Software compensator
- Circuit compensator

Now, we are going to present works that are related to these three compensation methods.

### **Compensation by modification on geophone structure**

In [11], the author proposed force feedback method to compensate geophone response in low frequencies. In this method, the inducted current in half of the coil is amplified outside the geophone and fed to other half of the coil. This current forces the coil to stay fix in the magnetic field. The simulations in [12] shows that the force feedback method can reduce the corner frequency to around

1  $Hz$ .

In [13], the authors proposed to add an external coil to the geophone to compensate the low frequency response. The concept is similar to force feedback method, but the reverse direction current is generated by the external coil.

Although both above mentioned methods could successfully compensate the geophone response in low frequencies, they have a major drawback. As mentioned earlier in this chapter, for SHM applications, we need to use an array of sensors. It means we need many geophones with modified body or coil. Moreover, we need to calibrate the geophones after modification to have reliable results.

### **Software compensation**

In all of the software compensation techniques, the compensator needs the digitalized data. Therefore they need to get the data from the ADC and then the compensator will run on the gathered data. The operation can be a level of a digital filtering or a software that estimate the response of the geophone in low frequencies.

In [14] the author used geophones which has corner frequency between 4  $Hz$  to 12  $Hz$ . Using a method called digital response improvement, the authors captured the vibrations two decades below the corner frequency. The compensator in this research paper is based on the real time discrete Fourier transform on the digitized signal of the geophone. Different size of windowing in the transform minimizes the leakage on each segment of data. It is assumed that data is available but polluted by different kind of noise in the sensor system. Thus, filtering can reconstruct the low frequency response. The problem with this method is the assumption of the availability of data. In cases that the data is below the noise level of the analog subsystem, the vibration information cannot be detected by this method. The other problem with this method is the computational power that the sensor system needs to for the real time DFT, correction, and the inverse DFT on the sampled data.

In [15] the authors used a software method to retrieve low-frequency response of a geophone with the corner frequency at 10  $Hz$ . Inverse filtering method that has been proposed in this research work is implemented inside the software. This type of filtering that will be discussed later in this section can either be implemented in hardware and software. The assumption that the author mentioned in this paper is that the self-noise of the sensor is significantly low. Therefore, the system does not amplify the noise of the signal in low frequencies. This assumption is practically unacceptable when we want to measure the environment with a low level of vibrations (i.e. basement of a building). Similar to the previous method, the other problem is that the author ignored the noise related to the analog subsystem and the ADC.

The main drawback of the software compensation techniques is that they already lost the part of the signal which is below the noise floor of the analog conditioning system. Therefore, instead of reconstructing the lost signal, they have to statistically predict the lost information.

## Circuit compensator

[16] shows another application of geophone which is surveying deep structures. In this research, the compensator circuit is mainly designed and optimized by the genetic algorithm. The fitness function for the genetic algorithm in this work gives more points to the design with a wider bandwidth. The final iteration of the genetic algorithm results in a feedback circuit with lower corner frequency compared to the geophone without response compensator. The problem here is that the genetic algorithm is a heuristic method. Therefore, each time running the algorithm may result in the different netlist for the circuit and different values for the components.

Besides the genetic algorithm, the only analog technique that has been proposed in several research works and patents is inverse filtering.

[17] is a patent that presents a circuit method to compensate the geophone low frequency response as well as amplifying the weak signal of mass-spring seismometers. The circuit that has been proposed in this research work is a variable gain amplifier. A non-inverting op-amp amplifier with three components in the feedback is responsible to change the gain of the amplifier. To prevent saturation in near 0 Hz, a series resistor is always in the feedback loop. The other components are a resistor in parallel with a capacitor. The combination of the capacitor and the resistor in the feedback causes variable gain for the amplifier circuit. Similar to other inverse filtering method, the total transfer function will be a function of the internal components of the mass-spring sensor.

In [18] the author extends the concept of the compensator for the geophones and galvanometers (which both using mass-spring in their structure). First, the author estimated the coefficients of the geophone voltage transfer. Then using the feedback method in the loop, they could set the total gain of the system as a function of input frequency. For the first version, the system is not stable at high frequency. Therefore, they moved toward the next version which is stable in a wider range of frequency. Again, the problem with this circuit is that the compensator does not have control over  $-3$  dB cut-off frequency of the total transfer function.

The inverse filtering technique is also presented in [7] as a method to improve the quality of output signal in geophones.

As we will see later in chapter 4, in all the inverse filtering techniques, the frequency response of the geophone after the compensation is still a function of the geophone physical characteristics. As a result, we do not have control over the whole bandwidth of the sensor.

## 1.4 Thesis Overview

Regarding the objectives of this research work, the thesis is organized as follows. Three different categories of sensors that have been used in this study are introduced in chapter 2.

In chapter 3, design procedure of a modern seismic sensor system has been discussed. This chapter includes the design specifications for a seismic sensor system and the details about all the modules that have been introduced in chapter 1 except the analog subsystem.

Analog subsystem for the seismic sensor is discussed in chapter 4. The main subject of this research work which is the geophone response compensator is a part of analog subsystem. In chapter 4,

besides a brief explanation about the amplifiers and filters, the proposed response compensator circuits have been discussed in details.

A set of test plans are defined in chapter 5 to evaluate the qualification of the proposed circuits and model in chapter 4. The tools and the equipment that are used for the experiments are also introduced in chapter 5.

Chapter 6 includes one test plan and measurements for a real building to evaluate the proposed techniques in a real environment.

The conclusions and the future possible works to improve the seismic sensor systems are in chapter 7.

## Chapter 2

# Seismic Sensors

The main component of each seismic sensor system is a seismic sensor. A seismic sensor generates a physical signal (i.e. voltage or current) regarding the motions of the body of the sensor.

In this chapter, we are going to explain three different sensors that have been used in this study.

### 2.1 Geophone (velocity meter)

Geophone is the only velocity meter that is used to the sensor system. Geophones converts the ground displacements to a voltage signal. The structure of a basic geophone is showed in Fig. 6.

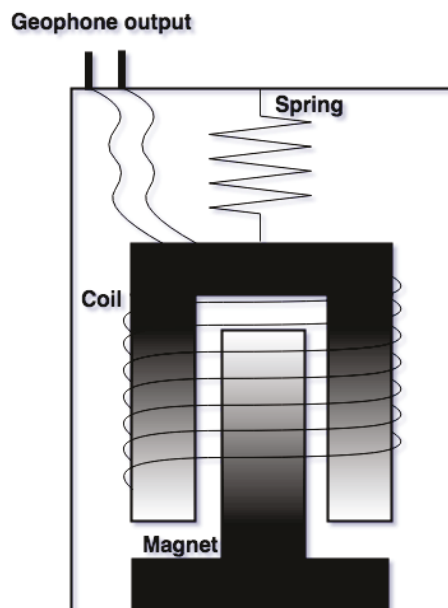


Figure 6: Geophone structure

The mass connected to the spring, fluctuates because of the vibrations of the body of the sensor. The spring moves accordingly. The moving spring being surrounded by a magnet is subjected to

an induced electric current by the principle of electromagnetism. The generated induced current in the geophone is proportional to the velocity of the mass. GS-11D from Geospace [1] is the geophone that has been used frequently in this study. Advantages and disadvantages of the geophone are as follow:

Advantages:

- Regarding the applications, geophones can be designed and built to operate over variety of frequencies and signal magnitudes.
- On the economic side, for the same price, geophones afford to more sensitivity compared to other types of sensors.
- Geophones are passive sensors and they do not need external power supply.

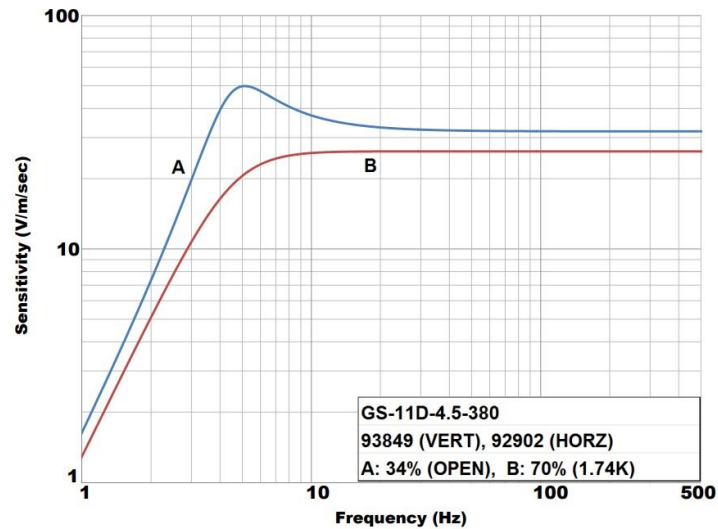


Figure 7: Frequency response of GS11-D for two different loads [1]

Disadvantages:

- The main disadvantage of the geophones is their response to vibrations at low frequencies, especially for frequencies of interest in SHM applications(see Tab. 1). Fig. 7 shows the frequency response of GS11-D with two different damping resistors. As we can see, the response is below the nominal 70% of the final response before  $\sim 4.5 Hz$ .
- Geophones are physically big and heavy. Geophones in different applications have different sizes and weights. GS11-D is one of the smallest available but still is many times bigger and heavier than a MEMS accelerometer. Moreover, each geophone can measure vibration in one direction. To sense movements in three directions, we need three geophones. Fig. 8 shows a housing designed for a three directions sensor. Note that the internal structure of the vertical geophone is different from horizontal geophones.

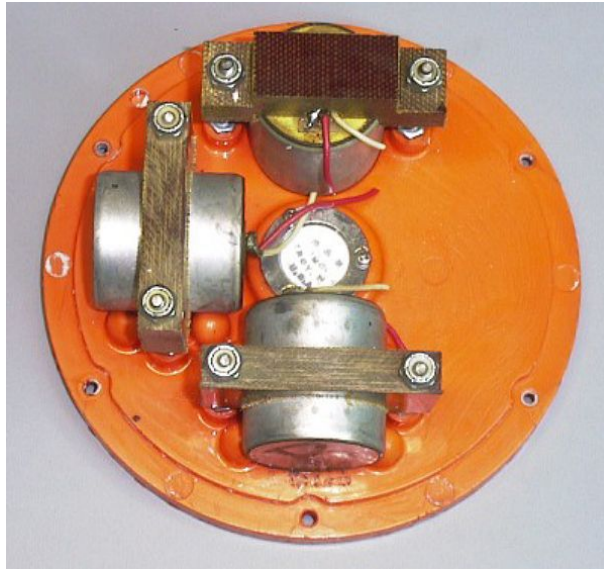


Figure 8: Housing for a three axis sensor system (photo from: [www.sydneystormcity.com](http://www.sydneystormcity.com))

## 2.2 MEMS Accelerometers

MEMS accelerometers are another type of sensors that have been used in many seismic systems. MEMSs have similar mechanism to the geophones but integrated into a single chip. In MEMS, layers of thin silicon and metal represent the mass and the spring. The internal structure of a MEMS accelerometer is shown in Fig. 9. The metal layer (shown as spring and mass in figure) is

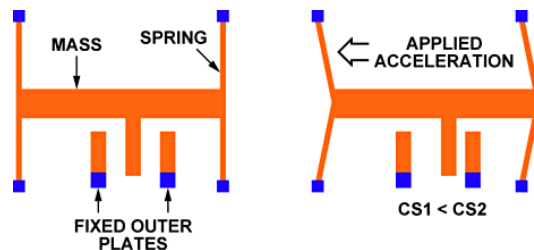


Figure 9: MEMS accelerometer internal structure

allowed to have a small amount of motions. When the layer moves, the capacitance of the sensor changes. The change of the capacitance can be converted to an analog data to represent the ambient acceleration.

ADXL-355 and ADXL-354 from Analog Devices [19] are two type of MEMS acceleameters that have been tested by our team.

Advantages and disadvantages of the MEMS accelerometers are as follow:

Advantages:

- Some MEMS accelerometers have integrated amplifiers and analog to digital convertors (ADC) which help to reduce the overall noise of the system and also are capable of interfacing directly

with the microcontrollers or microprocessors.

- MEMS are small in size and often have all three axes integrated into one chip.
- MEMS have a wider range of bandwidth in comparison with the geophones.

Disadvantages:

- For the same cost compared with geophones, MEMS accelerometers are not precise enough for use in seismic applications.
- As they are active sensors, they need external supply. For a precise result, the external supply must be regulated and filtered.

A part of the work of our team was to evaluate the feasibility of using MEMS accelerometers in seismic sensors. In [20], we compared the result of some vibration tests in a building with above mentioned model of MEMS accelerometer and a geophone.

## 2.3 Piezoelectric Accelerometers

Piezoelectric accelerometers are another category of sensors that have been used as the benchmark sensor in our experiments. Fig. 10 shows the internal structure of a piezoelectric accelerometer. The piezoelectric crystal inside this type of sensors changes the electrical polarization when it is mechanically stressed by the seismic mass that is located in top of the crystal. Piezoelectric sensors need a driver circuit to operate. The output of the driver circuit is a voltage proportion of the changes in the polarization of the piezoelectric crystal.

From the equivalent circuit of a piezoelectric sensor ([21]) it seems that the impedance function is of order three, in contrast with that of a geophone which is of order two. An extra processing by an integrator will be needed to produce the same kind of response as in a geophone. This extra processing step could account for a conversion of acceleration to velocity. Thus, the output response of both the devices could be the same physical entity (i.e. a displacement  $\sim$  electrical voltage). More detailed comparison between the geophone and the piezoelectric sensor is not available at this time, in open literature.

Advantages and disadvantages of the piezoelectric accelerometers are as follow:

Advantages:

- The piezoelectric sensors have flat response over the frequency of interest in SHM.
- After using the driver circuit, the output of the sensor does not need to any conditioning before digitizing the data.

Disadvantages:

- Similar to geophones, the piezoelectric sensors capture the vibration in only one direction. Therefore for a three dimensions sensor, we need three of them.

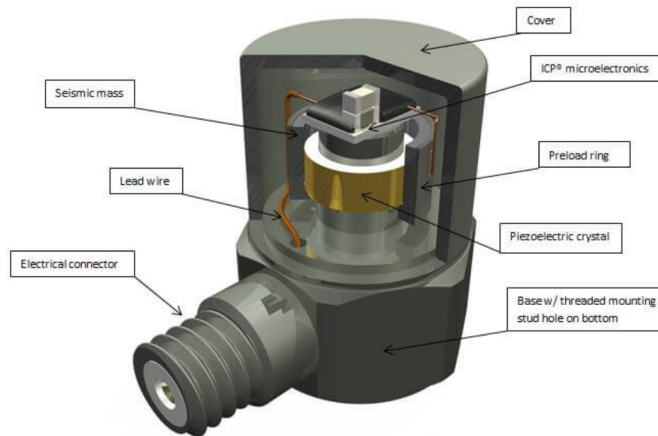


Figure 10: Piezoelectric accelerometer internal structure [2]

- The specific model that is introduced in chapter 5 is sensitive enough for applications in SHM. But the size of the sensor and the amount of power that it consumes make it impossible to use it in portable applications.
- Piezoelectric sensors have the highest price compared to other types of sensors.

## 2.4 Some important functional parameters of vibration sensors

In the following we discuss several functional parameters of a vibration sensor that are important in SHM applications. Also, these parameters helped us to choose the optimum sensor among all the available sensors.

### 2.4.1 Sensitivity

Sensitivity in general is the minimum vibration magnitude that the seismic sensor can respond to. In some cases, sensitivity of the sensor is reported as the gain of sensor (i.e.,  $V/10^{-3} g$  for accelerometers). The range of measurable parameters for several situations is presented in Tab. 1.

Vibration excitation	Frequency range ( $Hz$ )	Displacement range ( $\mu m$ )	Velocity range ( $mm/s$ )	Acceleration range ( $\mu g$ )
Traffic: road, rail	1-80	1-200	0.2-50	2-100
Blasting vibration	1-300	100-2500	0.2-500	2-500
Machinery outside	1-300	10-1000	0.2-50	2-100
Machinery inside	1-1000	1-100	0.2-30	2-100
Earthquakes	0.1-30	$10 - 10^5$	0.2-400	2-2000
Wind	0.1-10	$10 - 10^5$	-	-

Table 1: Vibration related parameters in different situations [6]

The numbers in Tab. 1 can be useful in selecting an appropriate seismic sensor for a specific application.

### 2.4.2 Dynamic Range

Dynamic range is defined as the ratio between the largest and the smallest vibration that the sensor can handle. The smallest vibration is usually the ambient noise level. Generally, MEMS accelerometers have wider dynamic range in comparison to geophones. Availability of a sensor for an application with required dynamic range can considerably reduce the amount of required signal conditioning.

### 2.4.3 Linearity

This parameter defines a sensor's output characteristics over the full dynamic range. Ideally, it is desirable for the sensors to behave like a linear system. This point is one the weaknesses of the passive sensors that use mass-spring structure to measure the vibration.

### 2.4.4 Gain

The gain for a sensor is defined as the changes in the magnitude of the output generated signal (either current or voltage) to the measured quantity (either velocity or acceleration). This parameter is often indicates in the linear dynamic range of the sensor. The gain of a sensor cannot inform us about the smallest signal that can be detected by the sensor. So, we separated the gain and sensitivity in two different sub sections.

## 2.5 Sensor Selection for the Sensor System

Three sensors have been introduced in this chapter with their advantages and disadvantages. Regarding our design requirements, we had to choose the optimum sensor (or sensors) for our application in SHM.

The piezoelectric accelerometer that we have used is the only sensor that does not need any analog subsystem. The output voltage level is high enough to use the whole resolution of the ADC and the frequency response is flat in our frequency of interest. The problem with the piezoelectric sensor is the amount of power that it needs to operate. The driver circuit for the piezoelectric accelerometer needs a 24 *v* power supply with the adequate current to drive the sensor. It is almost impossible to have this amount of power in a portable sensor system. Therefore, we only used the piezoelectric sensor as a benchmark for our experiments.

Several MEMS accelerometers have been tested during this research work. We can divide MEMS accelerometers into two categories; analog and digital. The analog MEMS needs at least one amplifier while the digital MEMS can be used without analog subsystem.

The MEMS are generally less sensitive compared to geophones and are suitable for structures that have higher amplitude vibrations.

For the prototype sensor, we considered a digital MEMS as the secondary sensor for the system. The advantage is that we do not need any conditioning circuit for the digital MEMS.

Geophones are sensitive enough for SHM applications. As they are passive sensors, unlike the do not need regulated voltage to operate. The only weakness that they have is their attenuated response to the vibrations below the corner frequency. Therefore, if we address this problem, they would be the optimum choice for a sensor system with application in SHM. Thus, we selected the geophone as the primary seismic sensor for our system and tried to overcome their frequency response problem.

## 2.6 Chapter Summary

We introduced the seismic sensors that have been used during this research. After investigations on the advantages and disadvantages of each sensor, we selected the geophone as the primary seismic sensor for the sensor system. Also, a digital MEMS accelerometer has been selected as the secondary sensor for the sensor subsystem.

## Chapter 3

# Example of a Modern Sensor System

In this chapter, we are going to present the design flow of the sensor system. To start, we need a set of design specifications related to the sensor applications in SHM. The specifications determine which module to choose for the sensor system to gain optimum functionality. The high-level specifications are:

- The sensor has to detect and record vibrations of the structures within our range of interest which is  $0.1\text{ Hz}$  to  $100\text{ Hz}$  in our case.
- The sensor has to sample the analog data of three geophones for three directions at the same time.
- The data from all the sensors must be accessible through a wireless connection after the tests. Also, the recorded data has to be stored in the module itself as a backup in case of failure in wireless connection.
- All the nodes must be synchronized [22]. Therefore, the commands from the remote device can be executed at the same time. The sensors have to be synchronized through a wireless network because generally, the sensors are far from each other. To test a building, it is necessary to locate the sensors in different places on different floors of the building and the wireless connection have to be able to keep the nodes connected and synchronized in all possible situations.

To build a sensor system to meet all the above mentioned requirements, we need several modules to work together in an embedded system. Every embedded system, needs a processor that is responsible to manage the modules of the system. We have selected STM32L4+ series of the microcontrollers by ST microelectronic [23]. As we will see in the following sections, the microcontroller (MCU) is engaged in all the tasks. The evaluation board of the MCU that has been used for prototyping is shown in Fig. 11. All the required connections and pins are accessible on the evaluation board. We

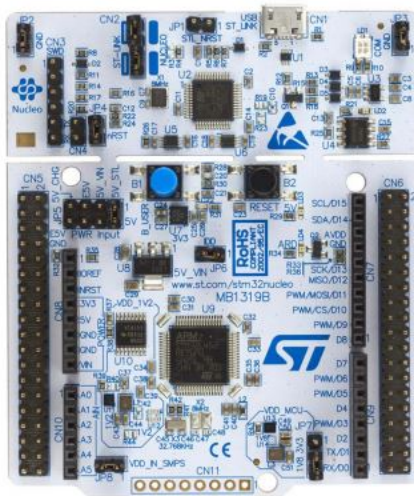


Figure 11: NUCLEO-L476RG Evaluation board of the MCU

are going to define three independent tasks for the sensor system. The tasks are:

1. Vibration recording
2. Wireless communication for data and commands transfer
3. Synchronization

In the following, we are going to explain each of these tasks and the modules that have been used in each task.

### 3.1 Vibrations recording

The vibration recording path is showed in Fig. 12. The seismic sensors that have been described in chapter 1 are three geophones located to measure the vibration in three directions and the digital MEMS accelerometer. The analog subsystem is explained in the next chapter. After receiving the start command, the MCU requests for data and determines the sampling rate of the MEMS internal ADC and the MEMS will start sending consecutive bytes in serial peripheral interface (SPI) protocol to the MCU. Also for the external ADCs, the MCU will request the ADCs to sample the geophone signal at a fixed sampling rate (144 sample pre second). LTC-2508 from Analog Devices [24] has been selected for the ADC in the sensor system. Clearly, we need three ADCs, but the problem with the multi-channel ADCs is that they have one sampling core and a multiplexer to choose from different analog inputs. Regarding our lab experiments, the switching delay for the input multiplexer is about  $15ms$  (for the only 24 bit multi-channel ADC at the time of the test) which is not acceptable in this application. Therefore, we used three single-channel ADCs. In case of using three ADCs, the MCU trigger the request to sample the analog signal at the same time and then will request to

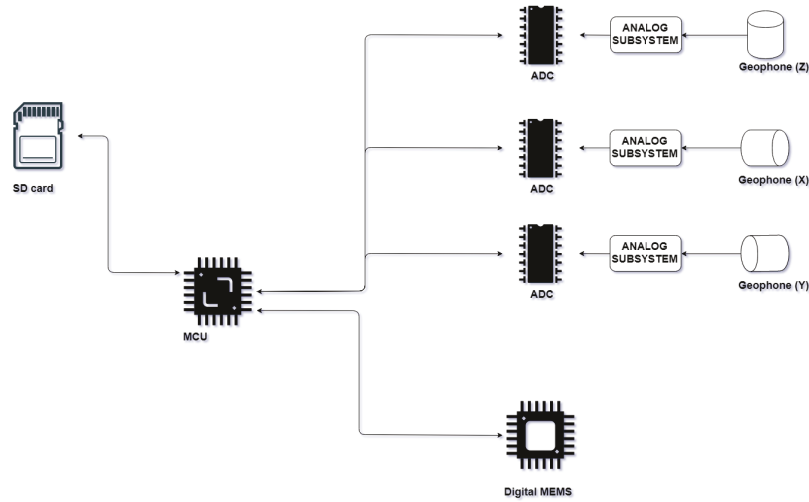


Figure 12: Modules that are engaged in the vibration recording

receive the stored data in the ADC’s internal register one by one. In this way, the ADCs sample the signal exactly at the same time but deliver the data to the MCU later.

ADC resolution is another characteristic of the ADC that we have considered during the design. LTC-2508 is a 32 bits ADC, however it is impossible to get the nominal resolution from the ADC. Effective number of bits (ENOB) is the parameter that determines the valid resolution of digitized data by the ADC. Note that the ENOB for the ADC which is always less than the nominal resolution of the ADC, mainly depends on the signal to noise ratio of the ADC [22]. ENOB for our case is measured 19-bits. It means 19 MSB bits of the recorded data by the ADC are valid and the rest are noise.

The communication protocol for both ADC and digital MEMS is SPI. The received data from these modules is stored in a large buffer in the MCU. After reaching a specific size, the MCU will store the data in the SD card in the format of a text file. The buffering mechanism is mandatory in this case, because the rate of the received data is far higher than the write speed of the SD card and it is impossible to read the data from the ADC and write it to the SD card byte by byte. Moreover, the time that it takes for the SD card to store one byte is the same as the time that it takes to write a page of data (64KB). Therefore, buffering data helps to save the MCU time.

### 3.2 Synchronization

In the previous section, we explained how the system samples and records the vibration data. Knowing that we need the vibration data of the structure from an array of sensors, we want all the sensors to start recording the vibration at the same time. This concurrency is mandatory to have a reliable dataset for the SHM specialist [22].

The other aspect of the synchronization is at MCU level. Suppose that we have different sensor systems with different precise crystals as the source of the clock for the MCU. Even if the crystals

have temperature invariant frequency, a slight difference in the frequencies for two sensors can result in different sampling rates for the two sensors.

Therefore, we need to address these synchronization problems. Fig. 13 shows the modules that have been used in the sensors for synchronization. To address the first synchronization problem, we

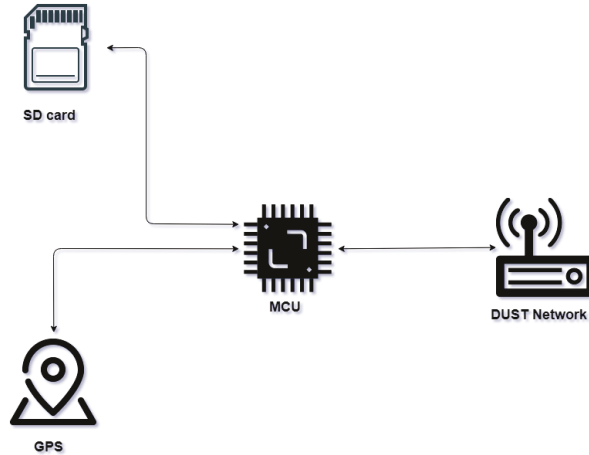


Figure 13: Modules that are engaged in the synchronization

tested some standard available local networks. After some tests, we have selected DUST network from Analog Devices [25] to keep the array of sensors synchronized. DUST is a module that provides a set of network functionality for the different applications. Fig. 14 shows the DUST kit that provided by the manufacturer to evaluate the module for our application. An internal MCU in each node of DUST provides an interface with a specific set of commands. These commands can be used by any external MCU or hosts (ie., a personal computer) to communicate with the DUST. In our case, the



Figure 14: DUST network kit for sensor evaluation

DUST is connected to the MCU via UART protocol. Based on the received data from the DUST, the MCU will make a decision for the operation. For example, at the start of a test, the host sensor broadcasts a signal to the network and waits for the acknowledge of other sensors. The host will broadcast the start command, when it receives the acknowledge from all the available sensors in the current test. Unless it repeats the broadcast and after a certain time, it will send an error message to the remote device that one or some of the sensors are not in range. In case of availability of all the sensors, an estimated delay for command propagation will be generated by the DUST. The MCU stores the delay in the SD card and labels test number. This delay can be used to compensate the start time drift in the software.

After the DUST evaluation, we need to mount DUST module on our board. Fig. 15 shows the DUST module that we have to mount on the prototype board. With the explained mechanism, the



Figure 15: DUST module to mount on the prototype board

array of the sensors is always synchronized for receiving commands from the remote device. We need to address the other problem which is the drift in the clock source frequency.

Different structures can be evaluated by the vibration sensors. In case of outdoor tests (ie., bridges), we can use a GPS module. Besides giving an accurate time and location label for the tests, a GPS module can provide an accurate pulse per seconds (PPS) signal. Using the PPS signal, we can accurately trigger an interrupt for the MCU clock source calibration at each second. Also, for indoor tests, we can generate a constant calibration factor for each crystal using PPS. Clearly, the calibration factor is unique for each sensor system and it is related to its oscillator. If we hardcode the calibration factor in the MCU firmware, we do not need to use GPS module each and every test. Fig. 16 shows the GPS module that has been used for the tests and prototype board.



Figure 16: U-blox NEO-M8Q-01A GPS module [3]

### 3.3 Wireless communication for data transfer

In previous sections, we explained how to get an accurate set of data with a synchronized array of sensors at the same time. The next step is to transfer the recorded data for the software analysis by the SHM specialists.

The stored data of the tests is available on the SD card of each sensor module, but in many cases, it is desirable for the user to access the data right after the test. A wireless connection is responsible for data transfer in these cases. Fig. 17 shows the modules that collaborate to transfer the results of the tests. During the tests, the MCU is busy to read and store the data from the geophones and the

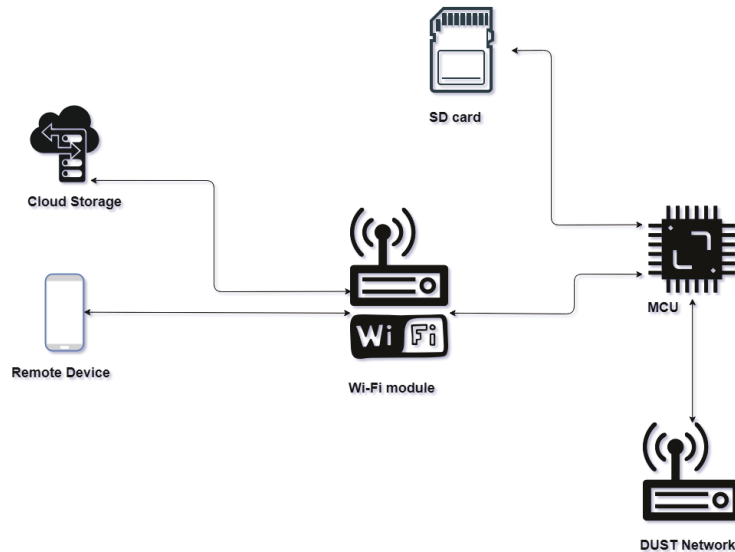


Figure 17: Modules that are engaged in the data transfer

digital MEMS accelerometer. Therefore, to prevent data lost, we have managed the data transfer to take place after each vibration test. When the test is finished, the MCU reads back the data from the SD card and sends it to the host sensor. Note that at this stage, only one of the sensors is responsible to communicate with the remote device. To prevent a collision in the DUST network, the sensors send the data one by one in a predefined sequence to the host. When the host received the data from all the nodes, it sends the data to the remote device (mobile phone or a PC) using WebSocket standard in WiFi communication. Fig. 18 shows SPWF04SA expansion board that has been used to prototyping. This board can be connected on top of the MCU evaluation board that has been shown in Fig. 11. The other alternative for the data transfer is to send the data to a cloud storage. This can be useful to monitor the structure under test from a long distance.

We explained the modules that are required to meet the specifications. The overview of these modules is shown in Fig. 19. There are other modules and mechanisms that are useful to have in a modern sensor system.

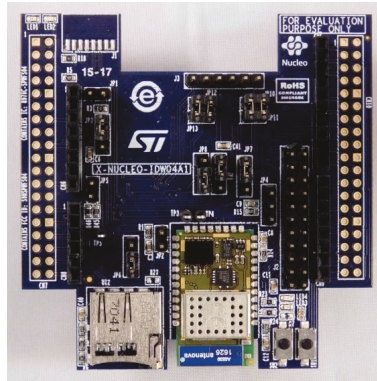


Figure 18: SPWF04SA expansion board for the Wi-Fi

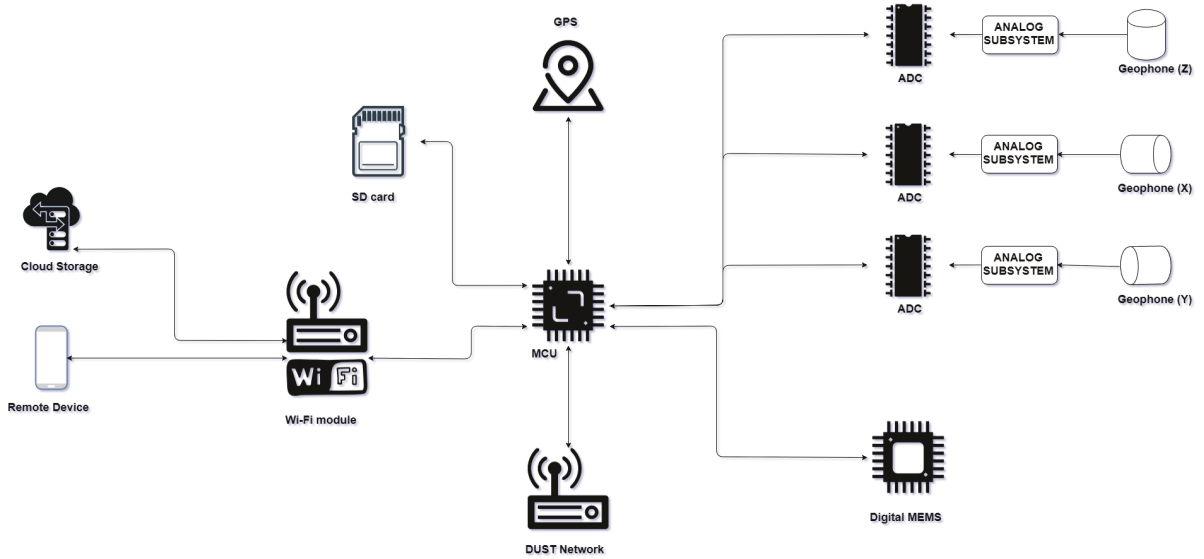


Figure 19: Sensor system overview

### Other operational modules

Power management system is the first item to mention in this section. Regarding the nature of the working environment, all the sensors are battery powered. Therefore, we have to consider a power management system to get the best of the batteries in the system. The power management system includes several regulators that are controlled by the MCU. The primary tasks of the power management is to supply different modules with different levels of voltages. Also, some of the chips in the sensor system need clean and stable voltage. For example, the reference voltage of the ADC must have certain isolation from other modules and ground. Power management system is responsible to provide this clean voltage for the ADC. Besides regulators, voltage monitor is another part of power management system. Its task is to report the voltage level of the batteries to the MCU. If the voltage of the batteries is below a certain level, the sensor warns the remote device to change(or charge) the batteries.

Based on the mode of operation, we need to supply the power for some of the modules. For example, during the tests, we need to power the ADCs, digital MEMS, SD card, and analog circuit for geophone signal conditioning (see Fig. 12). While we do not need the rest of modules, the MCU can shut down the supply for other modules to save the batteries power.

Protective relay is another module for the sensor system. The mass-spring structure of the geophones may generate a voltage even during the time that the sensor system is disconnected from the batteries. To prevent unwanted voltage in the circuits that can cause problems for the rest of the modules in the board, a set of relays have been considered in the design. The relays are normally closed and short the output of the geophone when the sensor is not in the operation mode.

### **3.4 Chapter Summary**

In this chapter, we presented the design flow of our target prototype for a modern vibration sensor system. The design start from defining a set of specifications. Then to meet each of the specification, we defined an independent task. To execute each task, some modules have been selected and managed to accomplish the task.

Next chapter includes the detail explanation of the analog subsystem as the main contribution of the author.

# Chapter 4

## Analog Subsystem

In this chapter, the analog subsystem for the seismic sensor system has been explained. Regarding the seismic sensor that has been used, the analog subsystem may include different circuits to shape and clean the signal. As an example, we do not need a response compensator for a MEMS accelerometer. Because the response of the MEMS accelerometers is flat in our frequency of interest. Response compensators, amplifiers, and filters are the main modules that have been used in this study. One of them, all of them or a combination of them can be used as the analog subsystem in the seismic sensor system. In Fig 20 two high-level diagrams of the possible circuits are shown. Analog subsystem (a) shows a setup using the inverse transfer function technique (this technique will be introduced later in this chapter) and analog subsystem (b) shows the setup that can be used for an analog MEMS accelerometer. In the following, the amplifiers and the filters that have been

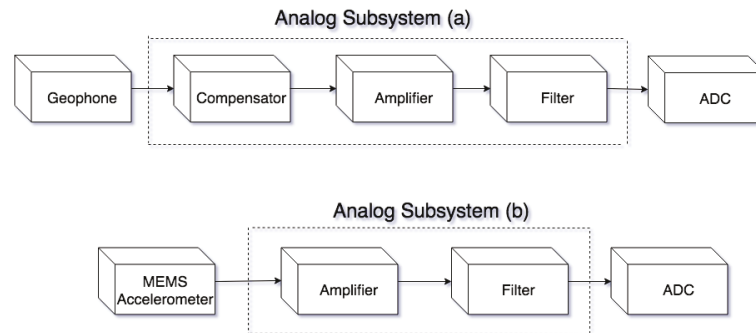


Figure 20: (a) analog subsystem for the geophone (b) analog subsystem for the analog MEMS

used in this study is briefly introduced. Then, several compensation techniques which are the main contribution of the author have been explained.

### 4.1 Amplifiers

The amplifiers are required to meet the total gain budget of the chosen analog subsystem. In other words, we need to cascade several stages to amplify and shape the analog signal before interfacing

with the ADC. Each of these stages has its own gain value. Multiplication of all these gains is the total gain of the analog subsystem. The total gain is important because we want the output signal of the analog subsystem to cover the whole range of operation of the ADC. The procedure of determining the required gain of the amplifier chain is explained in the following.

In [1] the sensitivity of the geophone has been reported as 32 volts per one unit of velocity in meter per second ( $m/s$ ). Considering the average of  $1 \frac{mm}{s}$  for the velocity of vibrations, for the ADC on hand we have:

$$\frac{ADC \text{ input range}}{\text{average velocity of vibration} * \text{geophone sensitivity}} = \frac{5}{1 * 10^{-3} * 32} = 156 \frac{v}{v} \quad (1)$$

Note that the input range of the ADC is 5 volts [24]. Therefore, a gain of 156 is required for the analog subsystem. The same procedure can be used for different combinations of ADCs and sensors. To achieve the above order of gain, we have tried the following alternatives:

- **instrumentation amplifier:** Instrumentation amplifiers are useful in cases where high gains are required for signals of the order of millivolts [4]. We have tried both integrated instrumentation amplifier (INA133 from Texas Instruments) and a discrete instrumentation amplifier using three op-amps (see Fig. 21).

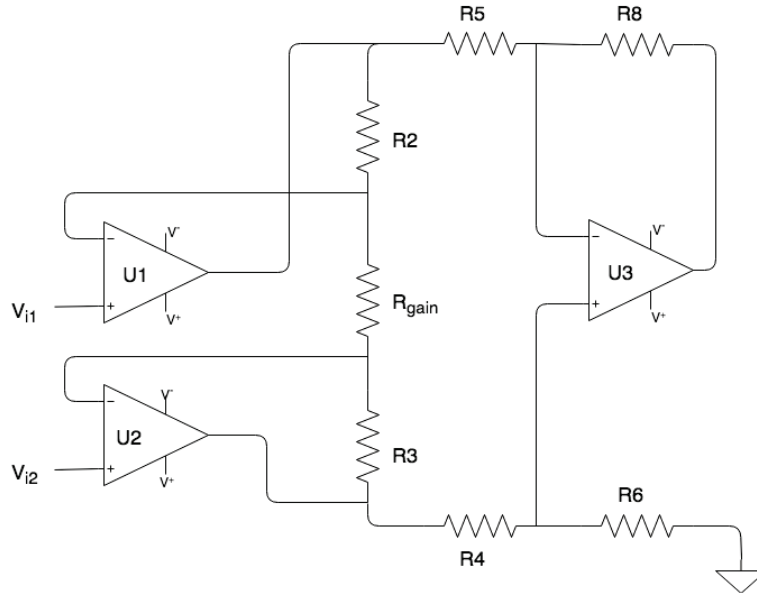


Figure 21: Instrumentation amplifier [4]

- **Non-inverting amplifier:** The work in [26] recommends using a non-inverting amplifier, as the first stage of the analog conditioning system. The reason behind this recommendation is that in case of using an inverting amplifier, the feedback resistor would load the internal coil of the geophone. This current will reduce the geophone sensitivity significantly.

As will see later in this chapter, only in some cases we need to use the amplifier. Because, the response compensators can adjust the gain. Therefore, we kept the differential amplifiers for the analog MEMS

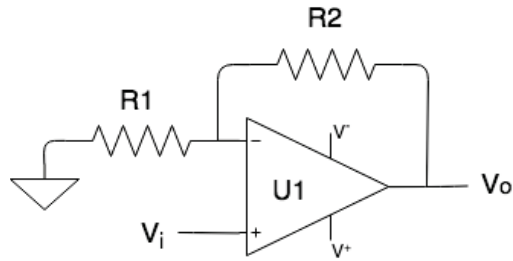


Figure 22: Non-inverting amplifier

and used non-inverting amplifiers to reduce the noise level [26] (as well as the complexity) for the analog subsystem when the amplifier is required.

## 4.2 Filter

A wide range of ADCs has been tested and studied to find the optimum choice for this application (more details are presented in Chapter 3). In all the models, an anti-aliasing filter is recommended to use by the manufacturer. The anti-aliasing filter is the last stage of the analog system before the ADC. Fig. 23 shows the  $RC$  filter that has been used for the ADC in differential mode. Note that for some compensation techniques, we could manage the output bandwidth and eliminate this stage from the design. More details are provided in the following section.

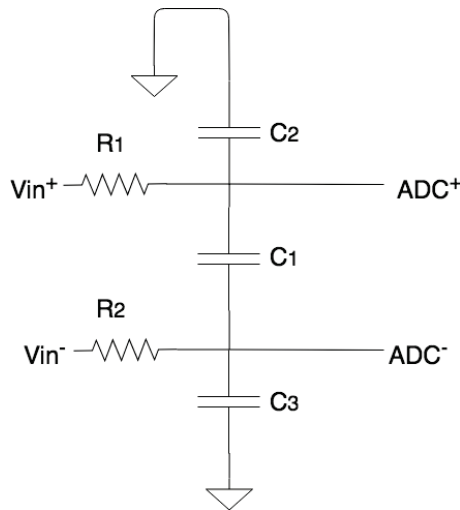


Figure 23: Passive RC filter for differential ADC

## 4.3 Frequency Response Compensator

The frequency response compensator plays a vital role in the sensor system quality. In the following subsections, several compensators that have been proposed in this study are presented.

Extensive simulations (PSPICE and MATLAB) were used to derive different configurations for the compensator circuits. For this approach to succeed, it is mandatory to work with an equivalent circuit model for the geophone.

In [5], the author has modeled the geophone based on its electrical and mechanical characteristics. Therefore, in the circuit model  $R_{equ}$ ,  $L_{equ}$  and  $C_{equ}$  are defined to model the mechanical characteristics and  $L_C$  and  $R_C$  are defined for the resistance and inductance of the coil. The geophone model using allocated components for coil is shown in Fig. 24. Practically, the first stage of the circuit after the geophone is a non-inverting amplifier. Therefore, the current that passes through  $R_C$  and  $L_C$  is negligible. Thus, we just represent the geophone using  $R_{equ}$ ,  $L_{equ}$  and  $C_{equ}$  in the circuit model that we have used for the circuit simulation.

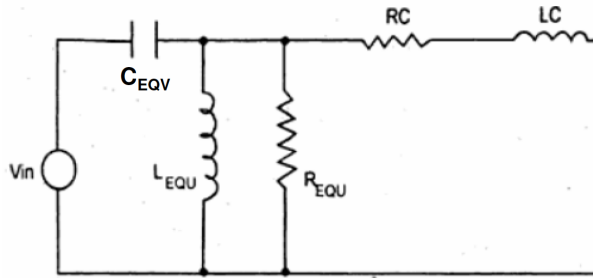


Figure 24: Geophone model with separated components for the coil [5]

As we can see in Fig. 7 from section 1.1.1 in chapter 1, the frequency response of the geophone can be modeled as a second-order high-pass filter. We used curve fitting techniques to extract the coefficients of the second-order high-pass transfer function as:

$$H_g(s) = \frac{s^2 + \frac{R_g}{L_g}s}{s^2 + s\left(\frac{R_g}{L_g}\right) + \frac{1}{L_g C_g}} \quad (2)$$

Note that the input of the transfer function represents the ground motions and the output represents:

- the current of the geophone with  $R_{Load} = 0$  in case of using the current source and
- the voltage of the geophone with  $R_{Load} = \infty$  in case of using the voltage source in geophone model.

The  $s$  in Eq. 2 is the complex angular frequency ( $j\omega$ ), where  $\omega$  is the  $\frac{rad}{sec}$  angular frequency. For GS11-D, the geophone that has been used extensively in this study, the values of  $R_g$ ,  $L_g$  and  $C_g$  are 380 *ohms*, 91.05  $\mu F$  and 2.78 *H*. The transfer function in Eq. 2, has an equivalent circuit representation as shown in Fig 25. Current source is more compatible with the nature of geophone as the current is induced to the center coil by the magnetic field. However, in some cases (i.e. circuit in Fig. 30), we have used the Thevenin's equivalent circuit of current model.

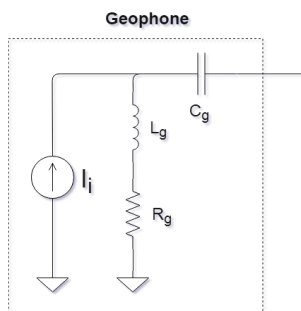


Figure 25: Geophone equivalent circuit with current source

Fig. 26 shows the circuit simulation result of the equivalent circuit in Fig. 25 using LTSpice. Our approach to the design of an optimum compensator is explained in the following.

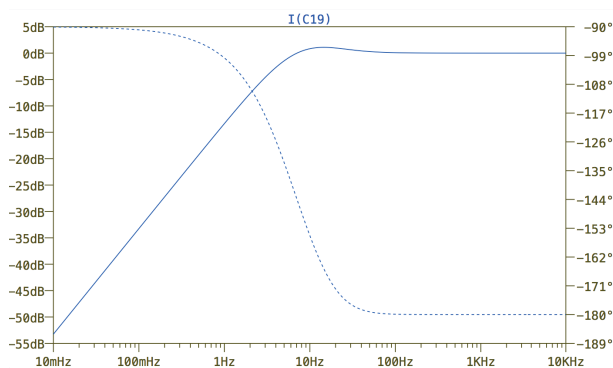


Figure 26: Geophone equivalent circuit simulation result. Magnitude (solid blue line) and phase (dashed blue line)

### 4.3.1 Passive Response Compensator

Generally, the output signal for the seismic sensors is of the order of millivolts. Using many components in the compensator and the analog subsystem will add more noise to the system. Therefore, the first step was to design a compensator using passive components.

Fig. 27 shows the structure of a passive compensator added to the geophone model of Fig. 25. To keep the design simple, we started with testing different  $RLC$ ,  $RL$ , and  $RC$  circuits. The best result is obtained by choosing serial  $R$  and  $C$  combination as the passive response compensator. Fig. 28 shows the circuit model for the proposed passive compensator.

Using numerical methods, we tried to find the optimum values for the  $R_1$  and  $C_1$  to obtain maximum backward extension of the  $-3$  dB corner frequency (see Fig. 28). In the simulations, we used values of  $R_1$  and  $C_1$  as the integer coefficients of the  $R_g$  and  $C_g$ .

Results of the simulations showed the maximum backward extension of the  $-3$  dB corner frequency

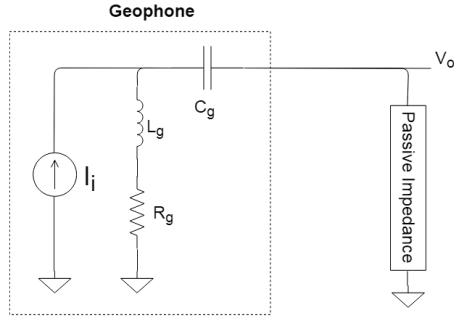


Figure 27: Passive compensator structure

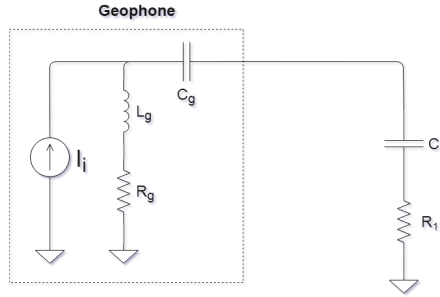


Figure 28: Passive compensator circuit

at:

$$C_1 = -2 * C_g \text{ and } R_1 = -1 * R_g \quad (3)$$

Fig. 29 shows the comparison between the response of the geophone (blue line) and the compensated response of the geophone using passive elements (orange line).

Two drawbacks of this technique are apparent. First, the negative value for the resistor and capacitor in Eq. 3 is only possible using active components. Second, the circuit could compensate for the limited low-frequency response of the geophone only by a small amount. Ideally, the response should be stretched backward until DC.

Conclusion that emerged from this part of the work is to try active circuit for the compensator.

### 4.3.2 Inverse Transfer Function Response Compensator

Re-writing the numerator of the geophone transfer function (Eq. 2) as:

$$H_g(s) = \frac{(s)(s + \frac{R_g}{L_g})}{s^2 + s(\frac{R_g}{L_g}) + \frac{1}{L_g C_g}} \quad (4)$$

We can see that there are two zeros in  $H_g(s)$ . At least one of the is responsible for the high-pass characteristics of the transfer function. Therefore, use of an integrator (i.e.,  $\frac{1}{s}$ ), and a lossy integrator

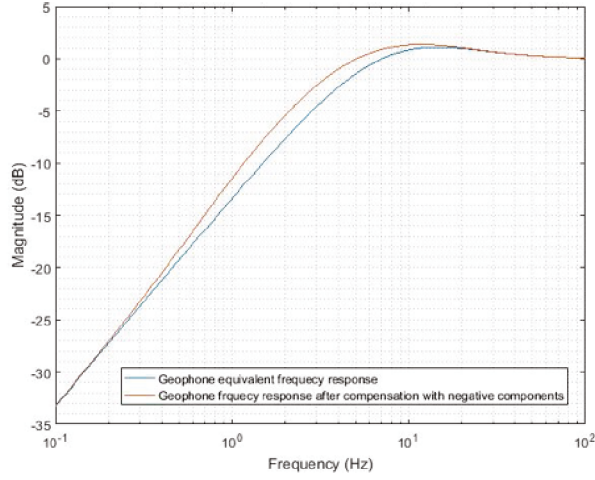


Figure 29: Passive compensator numerical simulation result

(i.e.,  $\frac{1}{s+1}$ ) can cancel out the zeros and convert the high-pass characteristics to a low-pass function of frequency. This is shown in Eq. 5.

$$H_e(s) = \frac{(s)(s + \frac{R_g}{L_g})}{s^2 + s(\frac{R_g}{L_g}) + \frac{1}{L_g C_g}} * \frac{K_1}{s + \frac{1}{C_1 R_1}} * \frac{K_2}{C_2 s} \quad (5)$$

In Eq. 5,  $\frac{K_2}{C_2 s}$  is the integrator and  $\frac{K_1}{s + \frac{1}{C_1 R_1}}$  is the lossy integrator. Fig. 30 shows the circuit that has been used in circuit simulations and experiments. Note that the values for the  $K_1$  and  $K_2$  can be adjusted to meet the total gain requirement of the overall system including the characteristics of the ADC.

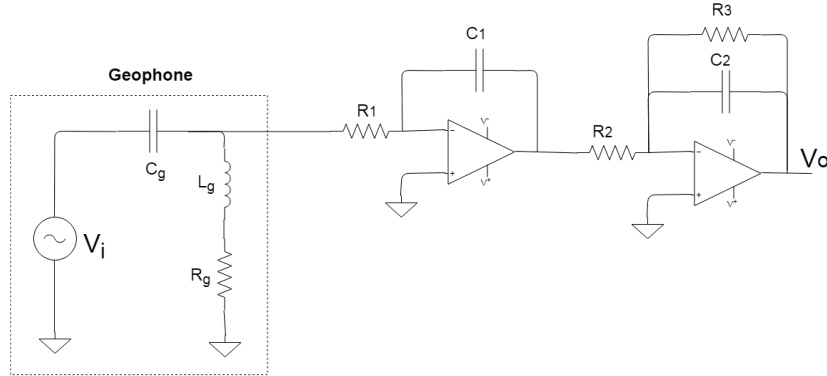


Figure 30: Circuit for inverse transfer function technique

Fig. 31 shows the numerical simulation of the  $H_e(s)$  in MATLAB. Clearly, the overall low-pass characteristic arises out of the natural components in the geophone itself.

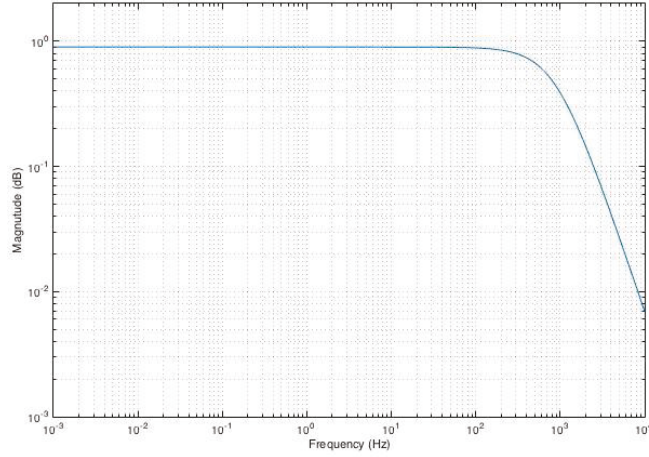


Figure 31: Inverse transfer function compensator circuit simulation

By adopting the inverse transfer function, the  $-3$  dB frequency remains dependent on the geophone parameters ( $R_g$ ,  $L_g$ , and  $C_g$ ). Therefore, as mentioned in section 3.1 in chapter 3, we might still need an extra anti-aliasing filter for the ADC. In order to realize the  $-3$  dB frequency independent of the natural components of the geophone device, the overall transfer function of the geophone plus the compensator need to include additional poles. This can be achieved by using multi-loop feedback principle in [27]. This is discussed in the following.

### 4.3.3 Multi-Loop Feedback Method for Compensation

Our objective is to create a low pass filter with adjustable cut-off frequency. The simplest transfer function that represents these characteristics is:

$$H_t(s) = \frac{K_0}{s + a} \quad (6)$$

$H_t(s)$  is the overall transfer function of the geophone cascaded with the compensator. To achieve this form, an unknown impedance box is considered in series with geophone. Unlike the passive compensator design, this time the impedance box can also include active components. (Fig. 32)

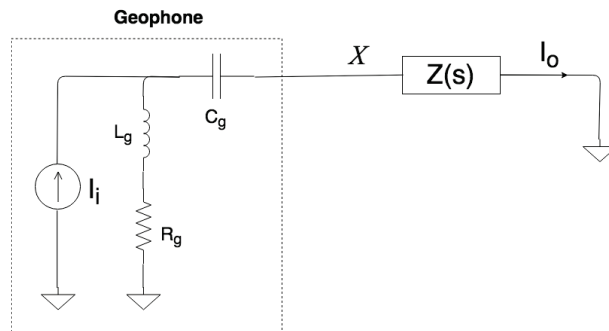


Figure 32: Geophone cascaded with an unknown impedance  $Z(s)$

The mathematical form of the circuit with the target function can be represented as:

$$H_t(s) = \frac{I_o}{I_i} = \frac{R_g + sL_g}{R_g + sL_g + \frac{1}{sC_g} + Z(s)} = \frac{K_0}{s + a} \quad (7)$$

To achieve the unknown active impedance, we solved Eq. 7 for  $Z(s)$ . The solution leads to:

$$Z(s) = \frac{s^3L_gC_g + s^2C_g(R_g - aL_g - K_0L_g) + sC_gR_g(a - K_0) - K_0}{sC_gK_0} \quad (8)$$

In Eq. 8, we assume that values of  $L_g$ ,  $R_g$  and  $C_g$  are fixed and we need to realize  $a$  and  $K_0$  to satisfy Eq. 7.

The  $Z(s)$  function can be realized as a voltage transfer function using functions of  $s^2$ ,  $s$  and a constant in series connection. This realization has the potential of increased noise levels at high frequencies. As an alternative to this problem, we can implement the admittance instead:

$$Y(s) = Z^{-1}(s) = \frac{sC_gK_0}{s^3L_gC_g + s^2C_g(R_g - aL_g - K_0L_g) + sC_gR_g(a - K_0) - K_0} \quad (9)$$

To design a circuit that represents behaviors of the admittance in Eq. 9, we used the procedure in [27]. Considering  $K_0 = 625$  and  $a = 625 \frac{rad}{sec}$  in Eq. 9, realization of the admittance  $Y(s)$  using ideal integrators is shown in Fig. 33.

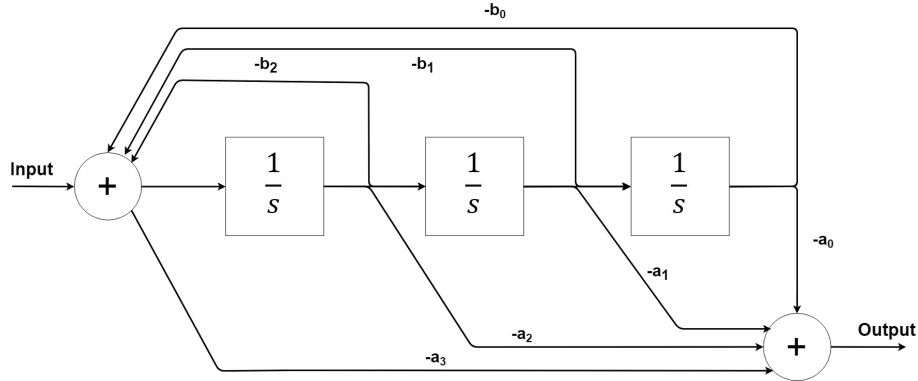


Figure 33: Realization of the admittance  $Y(s)$  using lossless integrators

Where the values of  $b_1$ ,  $a_0$ ,  $a_2$ , and  $a_3$  is equal to zero and the rest of values are as follow:

$$a_1 = \frac{1}{L_g}, b_0 = \frac{-K_0}{L_g * C_g}, b_2 = \frac{(R_g - 2 * L_g)}{L_g} \quad (10)$$

The system diagram of Fig. 33 can be implemented as the schematic diagram shown in Fig. 34. Note that the negative coefficients have been implemented using several cascaded inverting amplifiers. The arrangement of Fig. 34 is a voltage transfer function which present the scaled version of  $Y(s)$  in Eq. 9. Thus, Fig. 34 is a voltage transfer function ( $T(s)$ ) analogue of  $Y(s)$ . To realize the admittance in Eq. 9,  $V_o$  in Fig. 34 need to be passed through a transconductance amplifier. Further, to obtain an impedance from the admittance function, feedback is to be applied. This is displayed in Fig. 35.

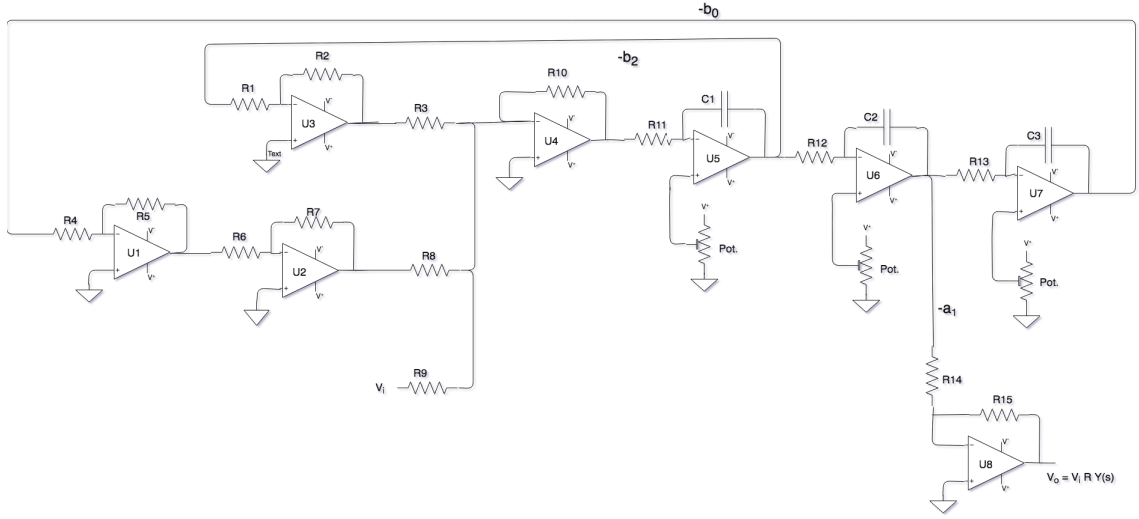


Figure 34: Schematic of  $T(s)$  analogue of  $Y(s)$  in Eq. 9

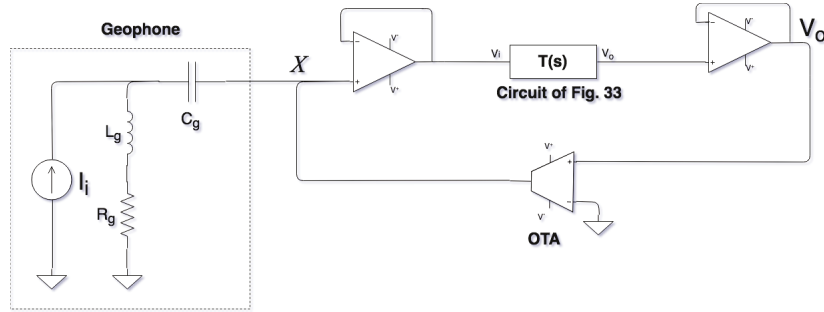


Figure 35: Admittance converter

To verify the work by the circuit simulations, we have used current source model of the geophone that is shown in Fig. 25. For the circuit simulation, as we expect, the result is a first-order low-pass transfer function. The result of the circuit simulation is shown in Fig. 36.

Use of integrators cause problems of the DC offset since that the integrator has infinite gain at DC. We had to use several potentiometers as of Fig. 34 to avoid saturation of the signal output.

Use of lossy-integrators to create the  $Z(s)$  function could obviate this problem. This, multi-loop feedback system with lossy-integrators could be a better solution for the compensator. This is discussed next.

#### 4.3.4 Modified Multi-Loop Feedback Method for Compensation

Using potentiometers to adjust the DC level of the signal may cause some problem for the product. Any mechanical shock for the sensor or unintentional touch of them by the human user may cause saturation for the op-amps and destroy the results of the entire test. To overcome these kinds of practical issues, we proposed using lossy integrator instead of the lossless integrator in the circuit realization of the impedance in Eq. 9. Therefore, in case of coming a DC signal, there is a resistor

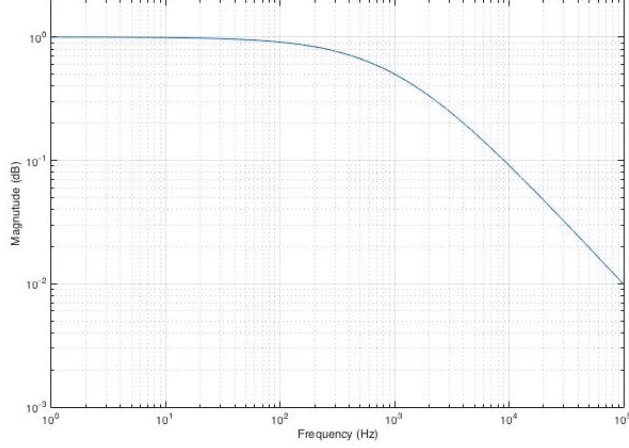


Figure 36: Circuit simulation result of the multi-loop feedback method for compensation

in the feedback of the op amp.

The design strategy for the modified multi-loop feedback method is similar to the ideal integrator based realization. Thus, we have the same target function that is shown in Eq. 6. To substitute the integrators, we need to start from the impedance in Eq. 9. The admittance  $Z(s)$  can be re-written as:

$$Y(s) = Z^{-1}(s) = \frac{(s + 1) + m_0}{(s + 1)^3 + n_2(s + 1)^2 + n_1(s + 1) + n_0} \quad (11)$$

The values of coefficients in Eq. 11 are as follows:

$$n_0 = \frac{-2\sqrt{\frac{R_g + 3L_g}{L_g}} - L_g - C_g - 1}{L_g}, \quad n_1 = \frac{2\sqrt{\frac{R_g + 3L_g}{L_g}}}{L_g}, \quad n_2 = \frac{R_g - 3L_g}{L_g}, \quad m_0 = -1 \quad (12)$$

Again at this point, we have the procedure similar to the previous method. The transfer function can easily be used to create the diagram of Fig. 37. This diagram defines the relations and gain of the lossy integrators with the input and output adders. The high-level diagram can be converted to

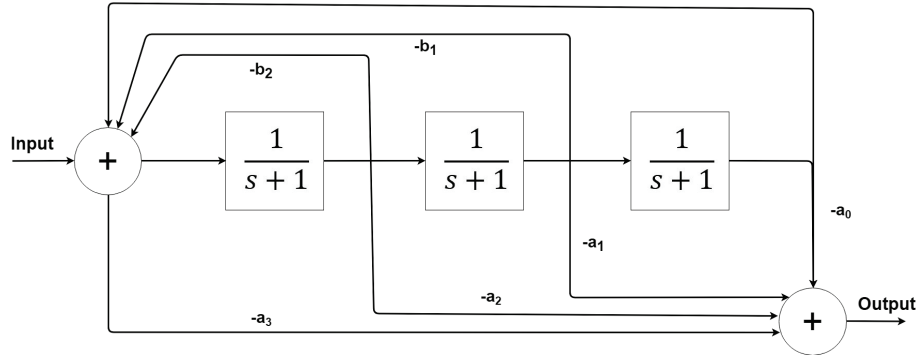


Figure 37: Realization of the admittance  $Y(s)$  using lossy integrators

the circuit shown in Fig. 38. Note that the negative coefficients of Eq. 11 are implemented using two

cascaded inverting amplifiers. Then using the circuit in Fig. 35, we converted the admittance to the

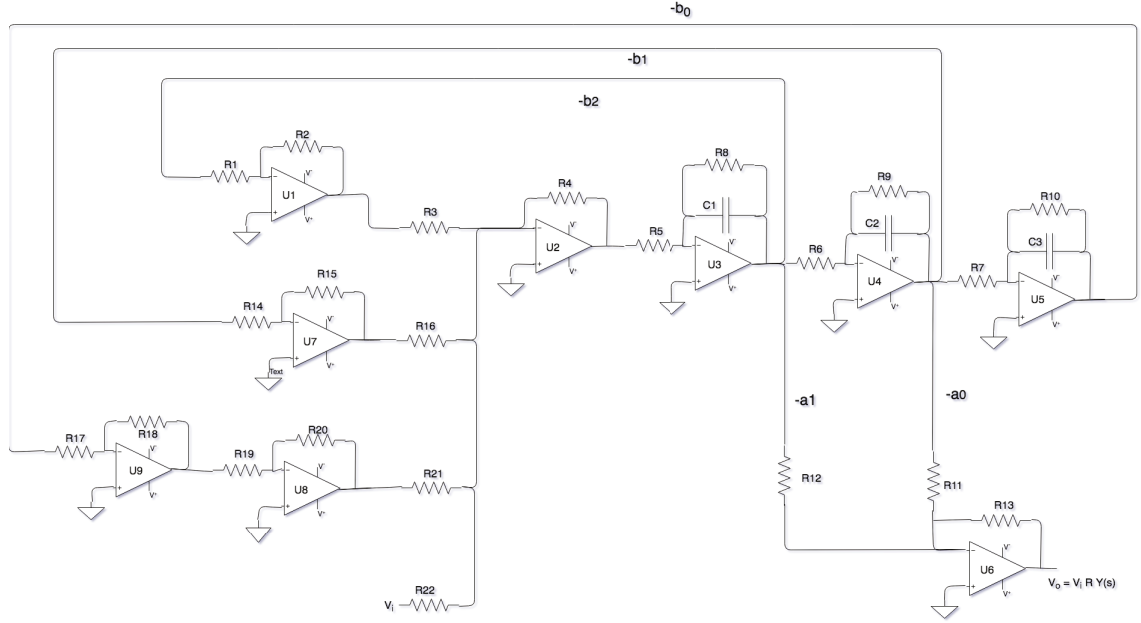


Figure 38: Schematic of voltage transfer function analogue of  $Y(s)$  in Eq. 11 using lossy integrators

impedance. As expected, the circuit simulation results is similar to multi-loop feedback transfer function method. The target function in both cases is a first order low-pass transfer function (see Eq. 6).

## 4.4 Chapter Summary

In this chapter, we explained the analog subsystem of our modern sensor system. Regarding the seismic sensor that is used in the sensor system, the analog subsystem may include compensator, amplifier, and filter or any combination of theses circuits.

Two structure for the amplifiers are described in the first section. The filter that is required for the ADC has been introduced. These two circuits are mandatory for each ADC interface to have clean and well shaped signal.

The next circuit that has been designed specifically for the geophone is the response compensator. Regarding the design specifications, we started with a response compensator with passive components. Then using active components, we proposed two different response compensators with different characteristics. The first technique is inverse transfer function. In this technique, an integrator and a lossy integrator eliminate the zeros in geophone transfer function. The second technique is multi-loop feedback method. This method changes the transfer function of the system to a target function. Therefore we have control over the bandwidth of the system after response compensation. The correctness of the proposed techniques in this chapter are verified by the laboratory tests as well as a test in the real building environment. These are described in the following chapters.

# Chapter 5

## Experimental Results

In this chapter, we are going to define different setups to verify the techniques that have been proposed in chapter 4. Also, the tools and equipment that have been used for the tests are introduced. In the last section of this chapter, the measurements are shown and the observations are discussed.

### 5.1 Test Plans

In following, four test plans are defined to verify the proposed geophone model and compensation techniques.

#### 5.1.1 Test Plan 1

The first test is arranged to verify the model that is used during the work for the numerical and circuit simulations. In Fig. 7 chapter 1, we saw the response of the geophone with two different loads. In this measurement, we target the open circuit response of the geophone to compare with our model presented in Eq. 2 of chapter 4. The reason behind choosing open circuit (or high impedance load) is that in the majority of tests, the geophone is connected directly to the positive input of op-amp in a non-inverting amplifier which has a high impedance.

#### 5.1.2 Test Plan 2

This plan is to verify the effectiveness of the inverse transfer function method that has been proposed in section 4.3.2.

In this experiment, we are going to compare the responses that are gathered from two setups in low frequencies (below the corner frequency). In the first setup, the geophone signal is amplified and filtered and then sampled by the ADC. For the second setup, the geophone output is compensated by the circuit presented in Fig. 30 in Section 4.3.2 of chapter 4 and then sampled by the ADC.

We need to excite the geophone at a certain frequency with the shaker that will be explained later in this chapter. For a fair comparison, both tests have identical situation except for the geophone conditioning circuits. The setup and two analog subsystems are shown in Fig. 39.

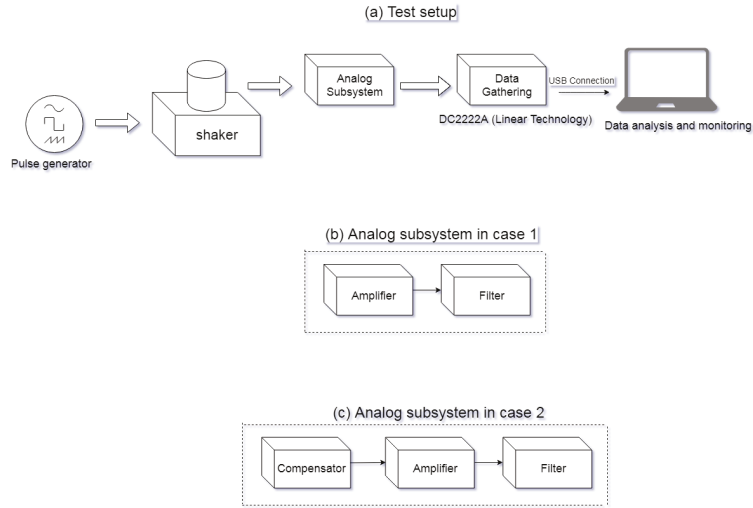


Figure 39: (a) Test setup; (b) Analog subsystem for case 1; (c) Analog subsystem for case 2

As we can see in Fig. 39, the received signal by the data gathering system is only amplified and filtered in case 1. In case 2, one additional compensation stage is also added to the analog subsystem.

### 5.1.3 Test Plan 3

In this test, we are going to verify the multi-loop feedback compensation method that has been proposed in section 4.3.3. The reason behind moving to this method is to eliminate the anti-aliasing filter that is necessary for the ADC. Therefore, besides the response on the low frequencies, we need to evaluate the compensator filtering effect.

The benchmark for this test is a piezoelectric sensor that is introduced in chapter 2. This is more sensitive than the geophone and has a flat response from  $0.07\text{ Hz}$  to  $300\text{ Hz}$  ([2]). Fig. 40 shows the piezoelectric sensor that we used for the tests. Note that we need a driver circuit for this sensor that is presented in [28].



Figure 40: Piezoelectric sensor

Fig. 41 indicates two setups that are used in this experiment. As we can see in Fig. 41, for the

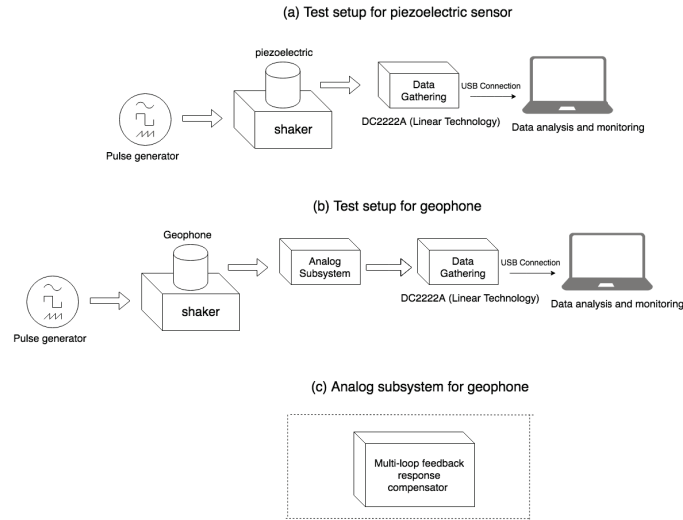


Figure 41: (a) Test setup for the piezoelectric sensor; (b) Test setup for the geophone; (c) Analog subsystem for the geophone (c)

geophone we only use a compensator circuit before the data gathering module.

#### 5.1.4 Test Plan 4

The last experiment is going to verify the modified multi-loop feedback compensator. As we use an identical target function for this method and multi-loop feedback method, we expect to see the same response from these two methods. Similar to the previous experiment, we compared the result of the modified multi-loop feedback method with a piezoelectric sensor. Again the comparison includes filtering effect and low frequency response compensation.

## 5.2 Equipment and Setup

In order to run the above mentioned tests, we need some laboratory equipment that are briefly introduced in this section. Fig. 42 shows the equipment in our electronics lab. All the equipment

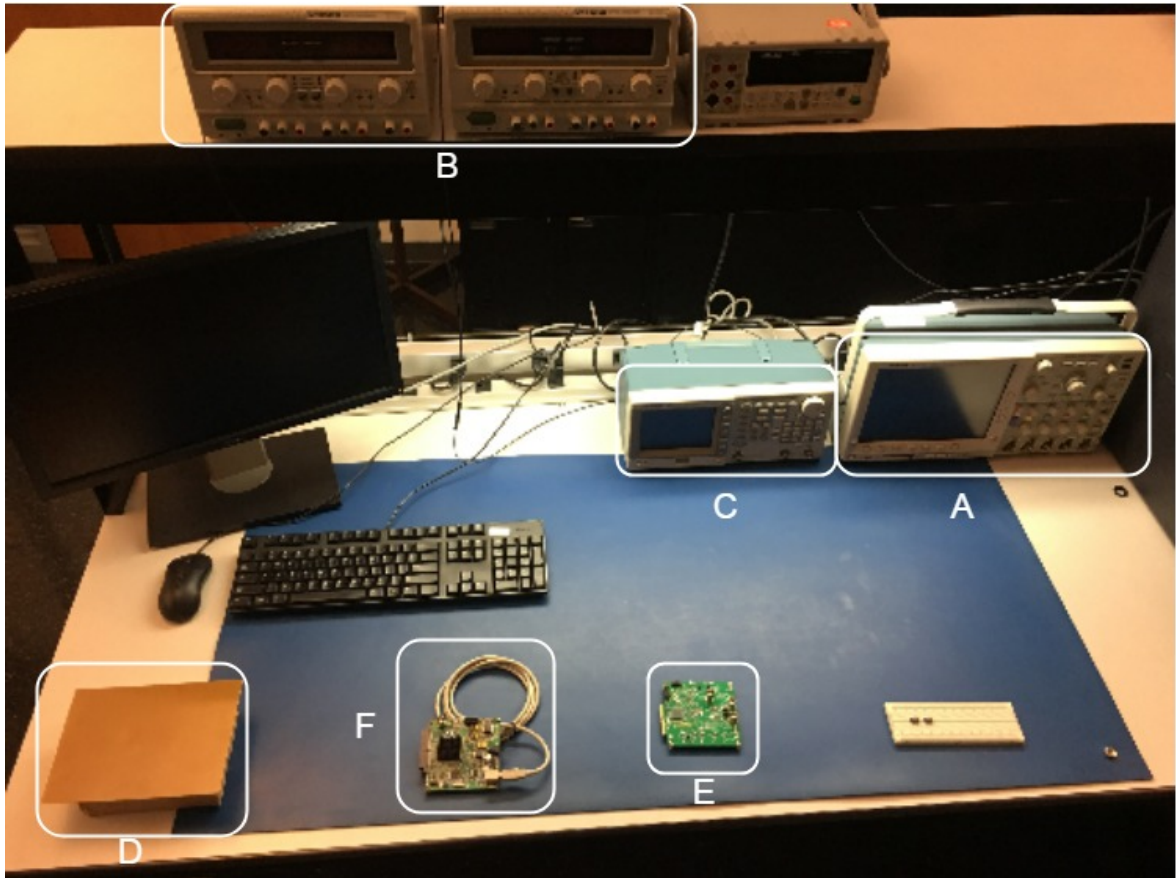


Figure 42: The lab equipments for the experiments

that are labeled in Fig. 42 are introduced in the following subsections.

### Oscilloscope

The oscilloscope is DPO-4104 from Tektronix. This device is used to monitor the signal from different nodes of the circuits mainly for troubleshooting purpose. The oscilloscope is labeled "A" in Fig. 42.

### Power supply

GPC-30300 from GW-Instek is the power supply that is used for the tests. As mentioned in chapter 3, a power management system is responsible to supply different modules and components in the sensor system. Therefore, before having the prototype board, we need to power up each module individually with different levels of voltages. During the experiments, up to three different power supplies have been used that are labeled "B" in Fig. 42.

### Signal generator

AFG-3101 from Tektronix is the signal generator that is used for the tests. We need one of them as the clock source for the data gathering system and the other one to feed a square wave to the shaker to hit the geophone at a fixed time interval.

The signal generator has also been used extensively in the primary stages of the study to test the ADCs, amplifiers, etc. The signal generator is labeled "C" in Fig. 42.

### Shaker

The shaker that is used for the tests was specifically built in the lab to excite the vibration sensors. The shaker structure is shown in Fig. 43.

A square wave signal from the signal generator is amplified with a power amplifier and drive a speaker. The speaker is fixed in a box. The unit under test on top of the box detects the hits at the edge of the square wave and generate a voltage related to the intensity and frequency of the hits. In this way, we can excite the sensors with vibrations in a wide range of amplitudes and frequencies. The shaker is labeled "D" in Fig. 42.

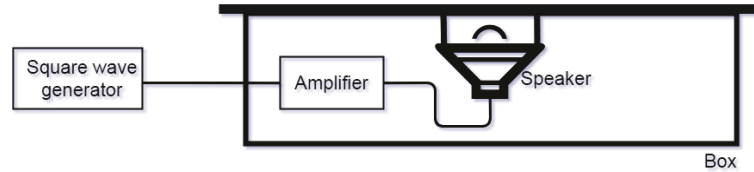


Figure 43: The Shaker structure

### Data gathering module

Data gathering modules for all the experiments was DC2222A-B from Analog Devices [29]. The ADC that is used in the prototype is LTC-2508 as explained before in chapter 3. DC2222A-B has a mounted ADC chip and also the voltage regulators and filters to deliver a clean DC voltage for the ADC power and the reference voltage. Fig. 44 shows the evaluation board of the ADC (left) and its interface board with the PC (right).

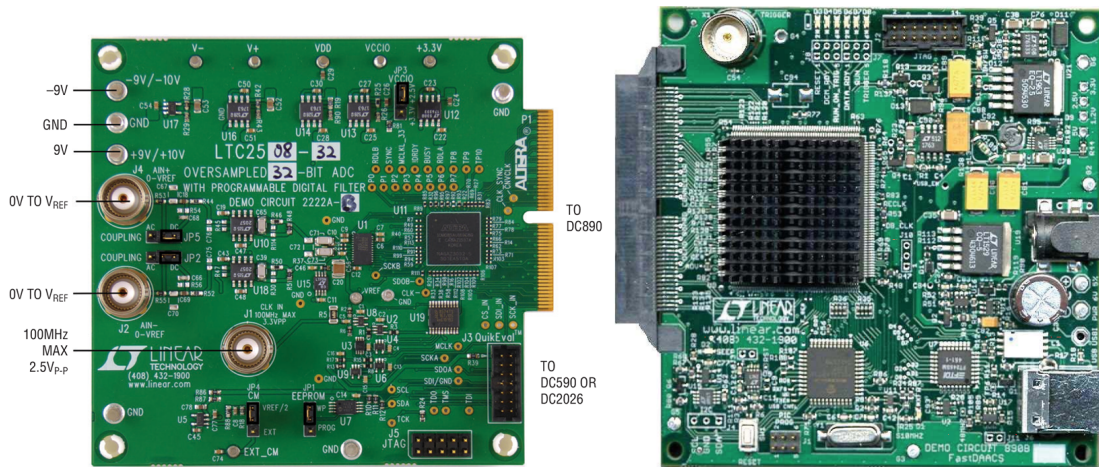


Figure 44: DC2222A-B: ADC evaluation board (left). DC890B: PC interface board (right)

The interface board with the PC is necessary to use the software package that is provided by Analog Devices. The software has the ability to visualize the data and also provides a text file including the ADC output data to use in other software (MATLAB). A screenshot of the software interface which is Pscope is shown in Fig. 45.

The ADC evaluation board and its interface are labeled "E" and "F" in Fig. 42 respectively.

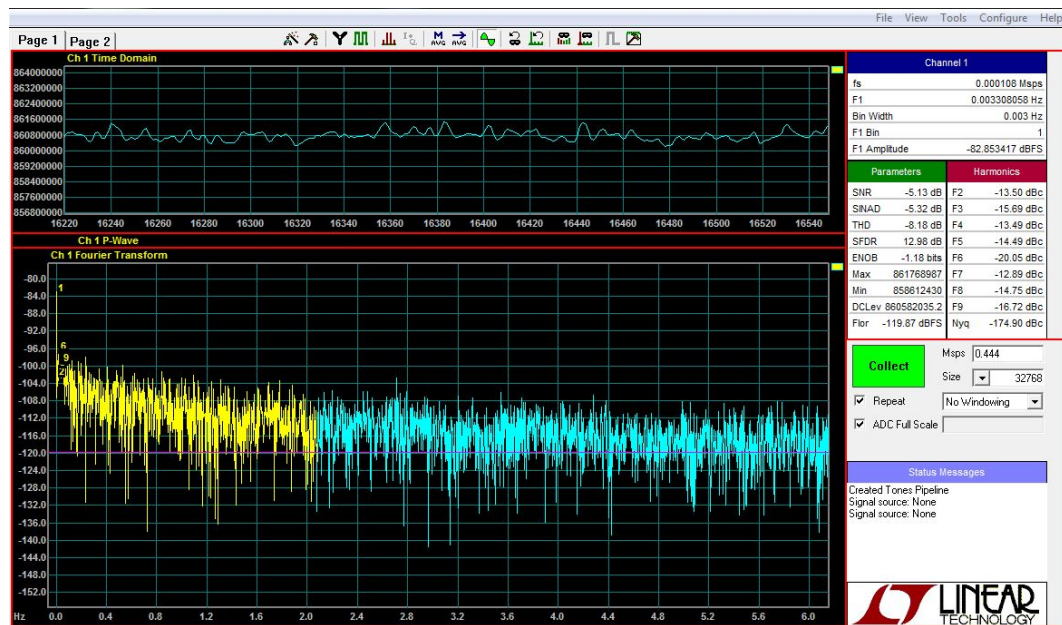


Figure 45: Screenshot of the Pscope software for a test

## 5.3 Measurements

Using the equipment that are introduced in the previous section, we are going to present the measurements.

### 5.3.1 Measurements for Test Plan 1

For the first test plan, we fed a 1 Hz square wave to the shaker. The geophone output includes the main frequency as well as all the odd coefficients of the main frequency (3 Hz, 5 Hz,...) within the geophone bandwidth. It happens because an ideal square wave can be presented as an infinite sum of sinusoidal waves. Eq. 13 shows the expansion of  $x(t)$  which is a square wave with the amplitude of 1 and the frequency of  $f$ . All the sinusoidal components of  $x(t)$  have  $(2k - 1)$  in their argument which represents an odd number.

$$x(t) = \frac{4}{\pi} \sum_{k=1}^{\infty} \frac{\sin(2\pi(2k - 1)ft)}{2k - 1} \quad (13)$$

Therefore, when we feed 1 Hz square wave to the shaker, we expect to get the response to all the odd coefficients of the main frequency as well.

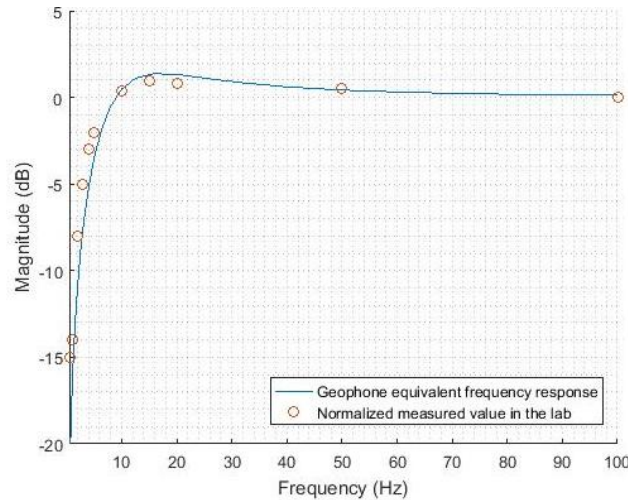


Figure 46: Geophone frequency response. Simulation vs. result of experiment

Fig. 46, shows the result of the numerical simulation (with MATLAB) of the geophone response (solid line) and the data from the real geophone (dots). The solid line in the graph is generate by MATLAB is the plot of transfer function that is shown in Eq. 2. For the real geophone, we excited the geophone with discrete frequencies by the shaker and measured the amplitude of the geophone while it is on the shaker (15 minutes for each test ). The normalized values of the measurements for discrete frequencies are shown by the dots in Fig. 46.

As we can see, the proposed model of the geophone which is explained in Section 4.3 of chapter 4 is qualified to represent the geophone in the numerical simulations.

### 5.3.2 Measurements for Test Plan 2

For the inverse transfer function method, first, we measured the response of the geophone without the compensator. Then, using exactly the same setup, we measured the compensated geophone response.

We repeated the test for two frequencies from the signal generator that fed the shaker. Fig. 47 shows the responses while the shaker is set to  $0.1\text{ Hz}$  and Fig. 48 shows the responses of the geophone for shaker in  $1\text{ Hz}$ .

In both Fig. 47 and Fig. 48, the blue line represents the compensated response of the geophone and the orange line represents the geophone response without the compensator.

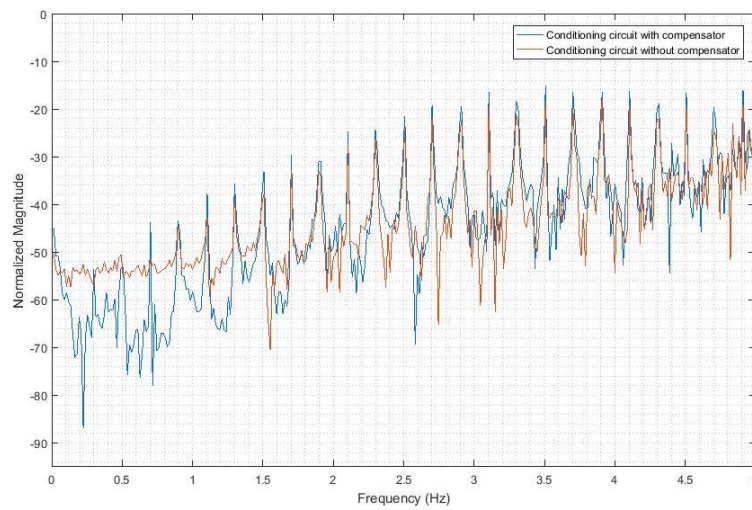


Figure 47: Compensated geophone Vs. geophone. Shaker at  $0.1\text{ Hz}$

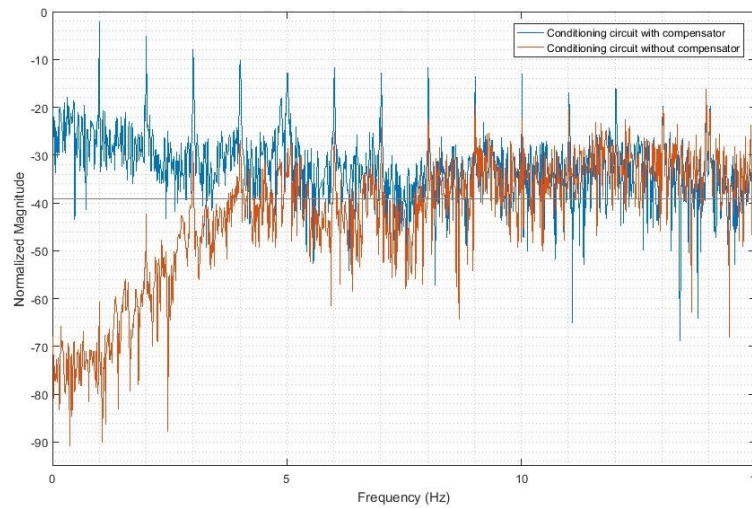


Figure 48: Compensated geophone Vs. geophone. Shaker at  $1\text{ Hz}$

In Fig. 47, the first vibration peak that is detected by the compensated geophone is at  $0.3 \text{ Hz}$  while the first peak for non-compensated geophone is at  $1 \text{ Hz}$ . The difference in the responses without and with the compensator is very clear in Fig. 48

### 5.3.3 Measurements for Test Plan 3

For the multi-loop feedback method, we have to check both the capability of the circuit on compensating the low-frequency response and tailoring the high-frequency noises to make the response appropriate for the ADC.

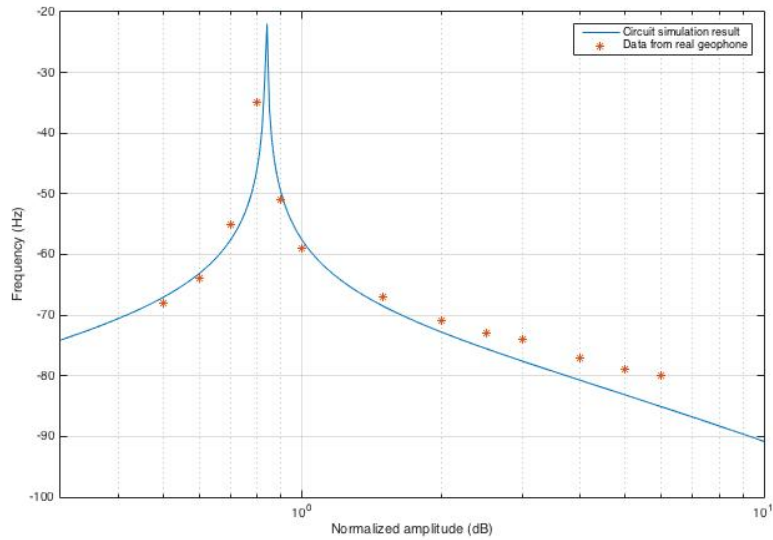


Figure 49: Impedance for the multi-loop feedback technique for geophone response compensator. Simulations vs. result of experiment

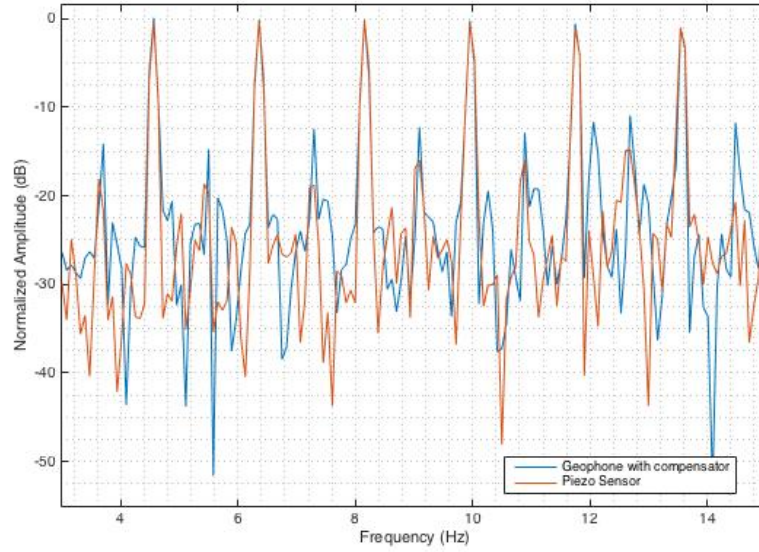


Figure 50: Compensated geophone vs. piezoelectric sensor response in low frequencies

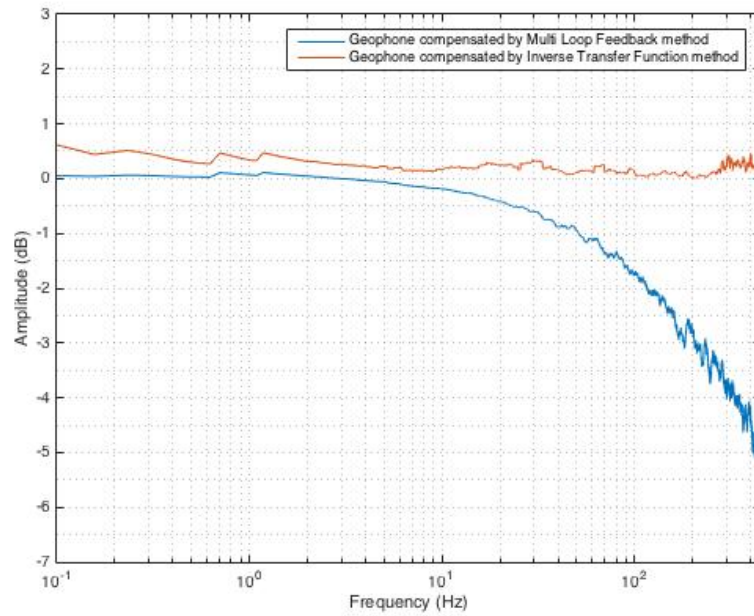


Figure 51: Filtering effect of multi-loop feedback method vs inverse transfer function method

For the benchmark sensor in the following tests, we have used a piezoelectric sensor. Piezoelectric sensors are generally more sensitive than the geophones and regarding their type have a flat response from 0.7 to 300 Hz [2]. For the first part of this experiment, we verified the correctness of the circuit presented in Fig. 34. We measured the values extracted from the circuit and compared them with

the circuit simulation results. The results are shown in Fig. 49. To get the circuit data, we used the signal generator to get the response of the circuit. In Fig. 49 the dots represent the results of measurements and the solid line represents the result of the simulation software.

Then we used the system in Fig. 35 to convert the admittance and connected with a geophone device (GS-11D) for vibration tests. Fig. 50 shows the responses of the compensated geophone system and of the piezoelectric sensor over a frequency span of DC to 20  $Hz$ . Clearly, the odd harmonics of the main frequency of the shaker is also visible in Fig. 50 as we used a square wave to feed the shaker. In the figure, the blue line represents the compensated geophone response and orange line represents the piezoelectric sensor response.

Before going to the next experiment, some clarification is required. In all the experiments, practically we have two different sources of vibration. The shaker and the ambient vibration (building in our cases). The ambient vibrations constitute an artifact signal. To gain an estimation of the ground vibrations, we measured the response of the geophone on the test location and subtract it from our results to have a virtually flat response. Fig. 51 shows the smoothed result of the measurement from compensated geophone and the piezoelectric sensor in a wider range of frequency compared to that in Fig. 50. Also, the ambient vibration is subtracted from the result of both tests.

For this experiment, the clock source of the data gathering system has a small drift. The drift that has been explained in chapter 3 causes a frequency shift in Fig. 50.

The values of  $K_0$  is set to 625 and  $a$  is set to  $625 \frac{rad}{sec}$  for this experiment (see Eq. 6). Therefore, we expect to see 100  $Hz$  as the 3  $dB$  frequency of the low-pass transfer function of the compensated geophone in Fig. 51. But the measured cut-off frequency is  $\sim 110 Hz$ . The reason of the frequency shift is that it is almost impossible to have the exact values of calculated capacitance and resistance in the lab.

### 5.3.4 Measurements for Test Plan 4

In the previous experiment, we verified the multi-loop feedback method. For the modified version of this compensator, we changed the realization circuit of the admittance to the circuit that is shown in Fig. 38 and compared the measurements with the result from piezoelectric sensor. Fig. 52 and Fig. 53 show the results of the tests.

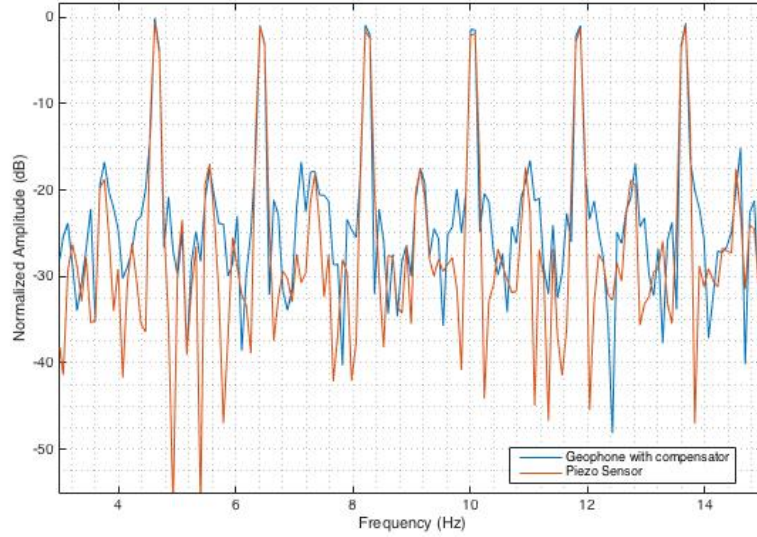


Figure 52: Compensated geophone vs. piezoelectric sensor response in low frequencies

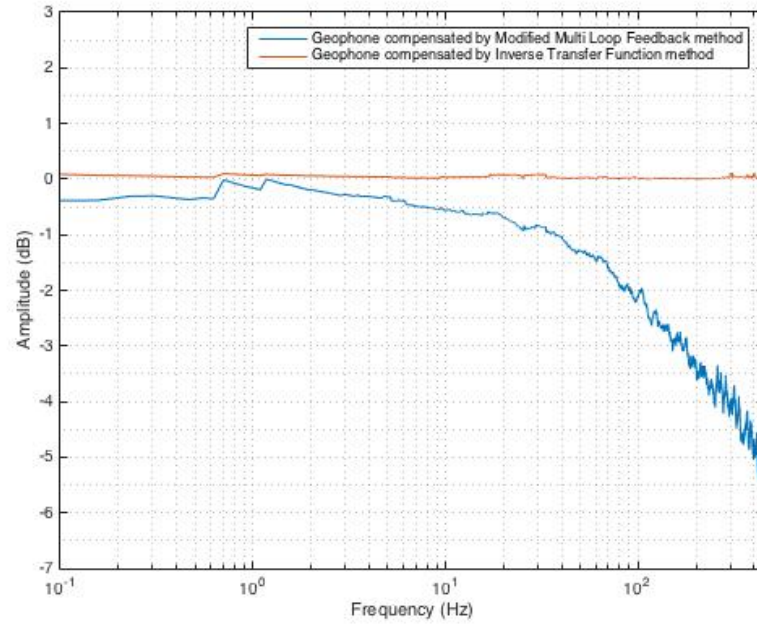


Figure 53: Filtering effect of modified multi-loop feedback method vs inverse transfer function method

The results show the effectiveness of the modified multi-loop method to compensate for the geophone response at frequencies close to DC and also complying with the expected low-pass corner frequency.

## 5.4 Chapter Summary

In this chapter, first we defined a set of plans to verify the proposed techniques in chapter 4 in the electronic laboratory. Then we introduced the tools and equipment that have been used for the experiments. Measurements for the defined test plans are the last part of the chapter. For each test plan, we either used the simulation results or the results of a benchmark sensor to compare the results. For all the experiments in this chapter, we used a shaker to excite the sensor at some certain frequencies. Next chapter includes the results of the tests for the real building ambient vibration without the shaker.

## Chapter 6

# Buiding Test

For all the tests in the previous chapter, we used a shaker. Using a shaker, we evaluated the compensated frequency response of the geophone in the frequencies below corner frequency. In this chapter, we want to test the proposed circuits in a real environment.

### 6.1 Test Plan

Regarding the information provided in Tab. 1, the effect of wind in buildings can start from  $0.1 \text{ Hz}$ . For the test, we considered four different locations on the sixteenth floor of Engineering and Visual Art building (EV building) of Concordia University (Fig. 54) For a valid data test in a building



Figure 54: EV building, Concordia University (from [www.concordia.ca](http://www.concordia.ca))

vibration test, the sensors must be triggered at the same time. Due to limitation in number of sensors, we measured the vibrations with one sensor in two directions (north and south). Note that the intensity of the vibrations may be different due the building structural design.

Similar to the experiments in the chapter 5 , we used the piezoelectric sensor as the benchmark for our sensor.

## 6.2 Measurements

Fig. 55 shows the plan of the 16th floor of the EV building. Five different locations in the plan have been considered as the test point for the building. We measured the vibrations in two directions; north-south and east-west (the north direction is shown in Fig. 55 by an arrow and the letter *N*).

The results of vibration test are shown in Fig. 56 to Fig. 60. Each figure shows the result of



Figure 55: The plan of 16th floor of EV building

vibration test for one spot in two directions. Five different spots are shown in Fig. 55 with red font. In each subplot of Fig. 56 to Fig. 60, the gray lines show the Fourier transform for the displacement data gathered by the compensated geophone (by modified multi-loop feedback method) and the black line is the Fourier transform of the displacement data gathered by the piezoelectric accelerometer. Clearly, the accelerometer data has been converted to the displacement before the Fourier transform.

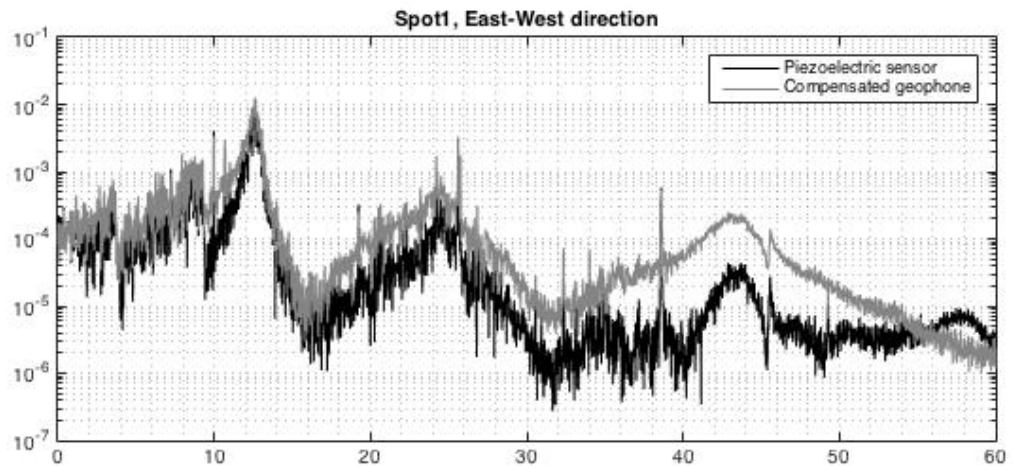
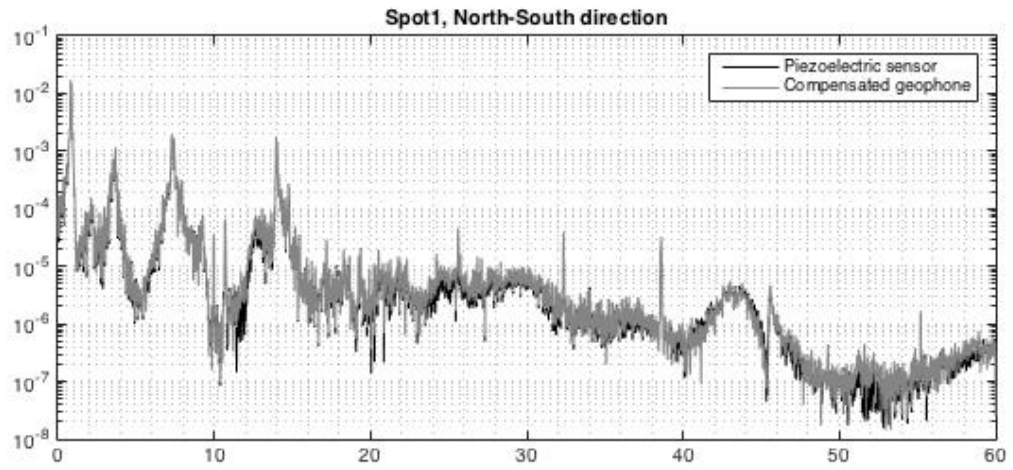


Figure 56: EV building vibration test in spot 1 (See Fig. 55)

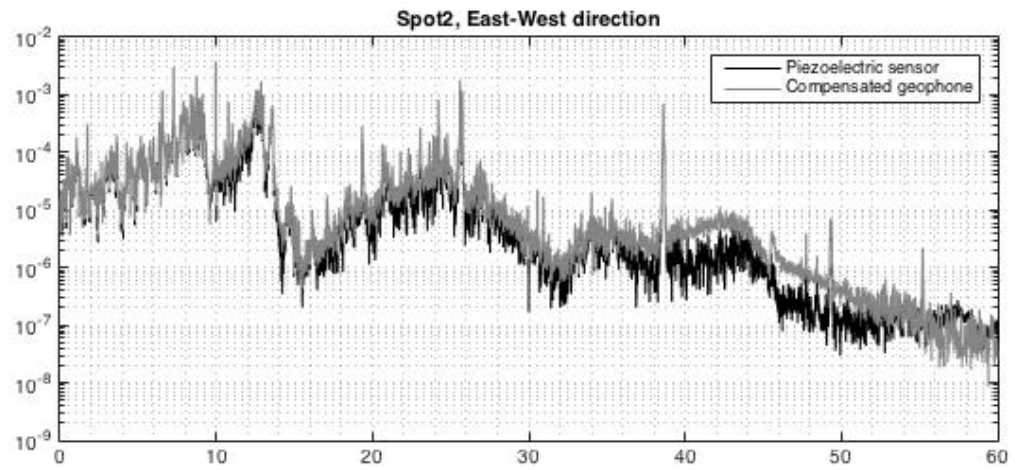
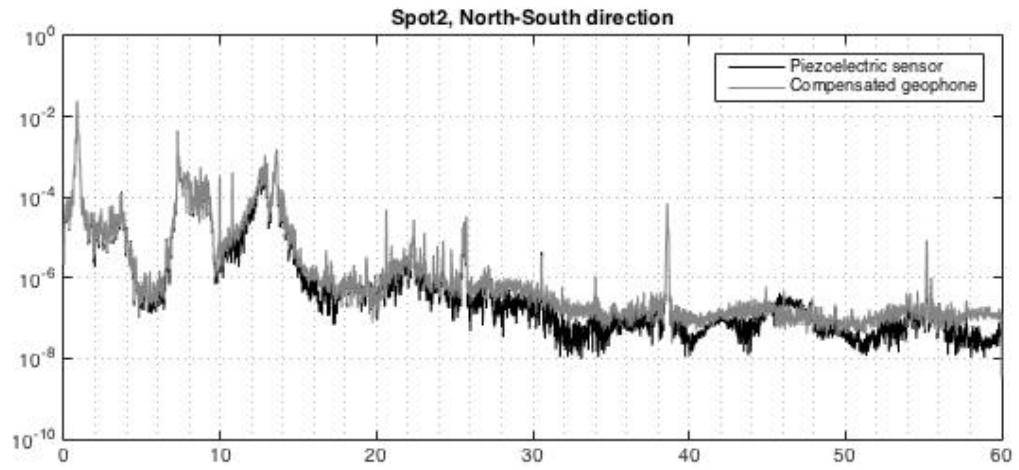


Figure 57: EV building vibration test in spot 2 (See Fig. 55)

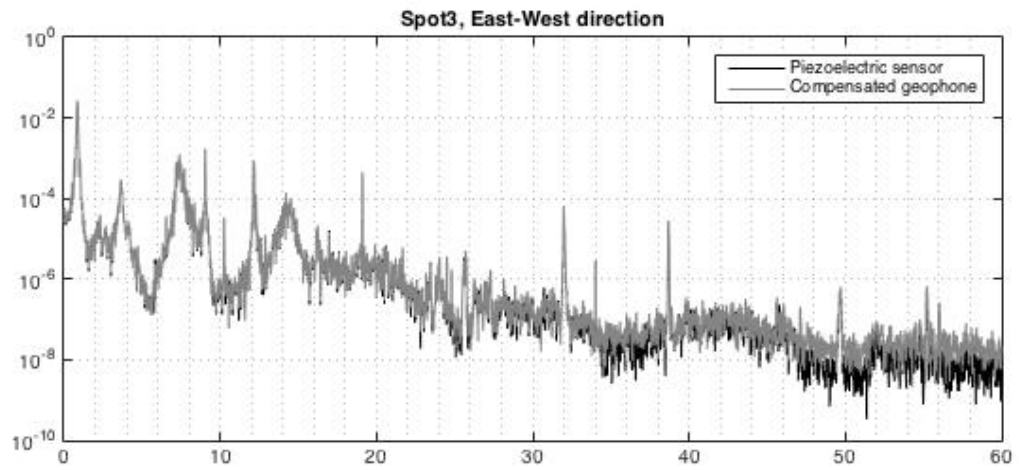
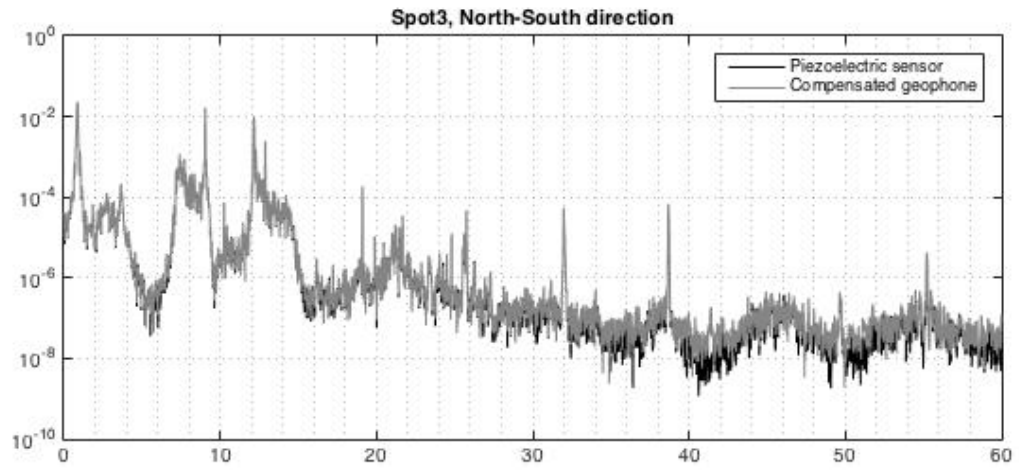


Figure 58: EV building vibration test in spot 3 (See Fig. 55)

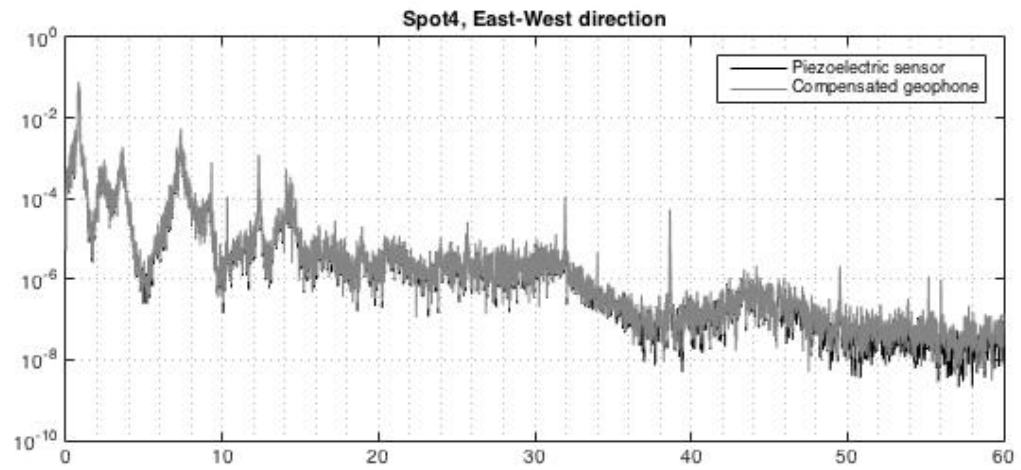
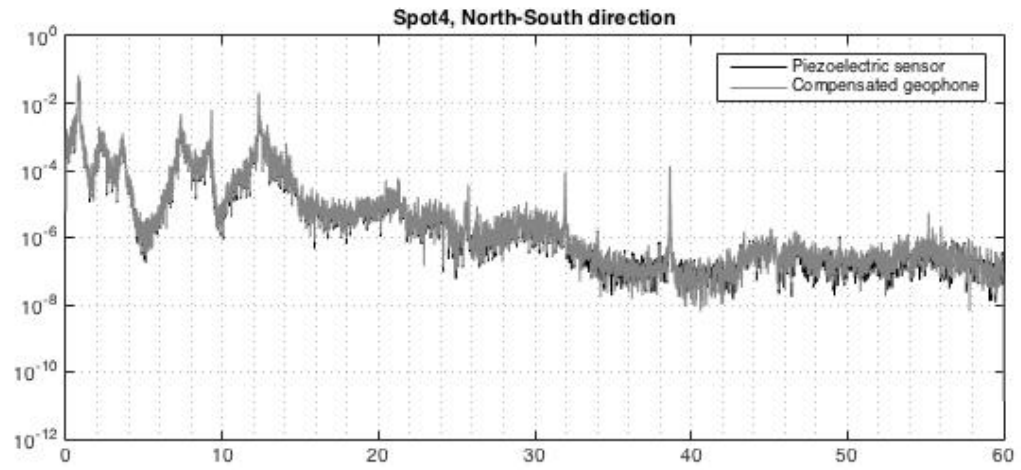


Figure 59: EV building vibration test in spot 4 (See Fig. 55)

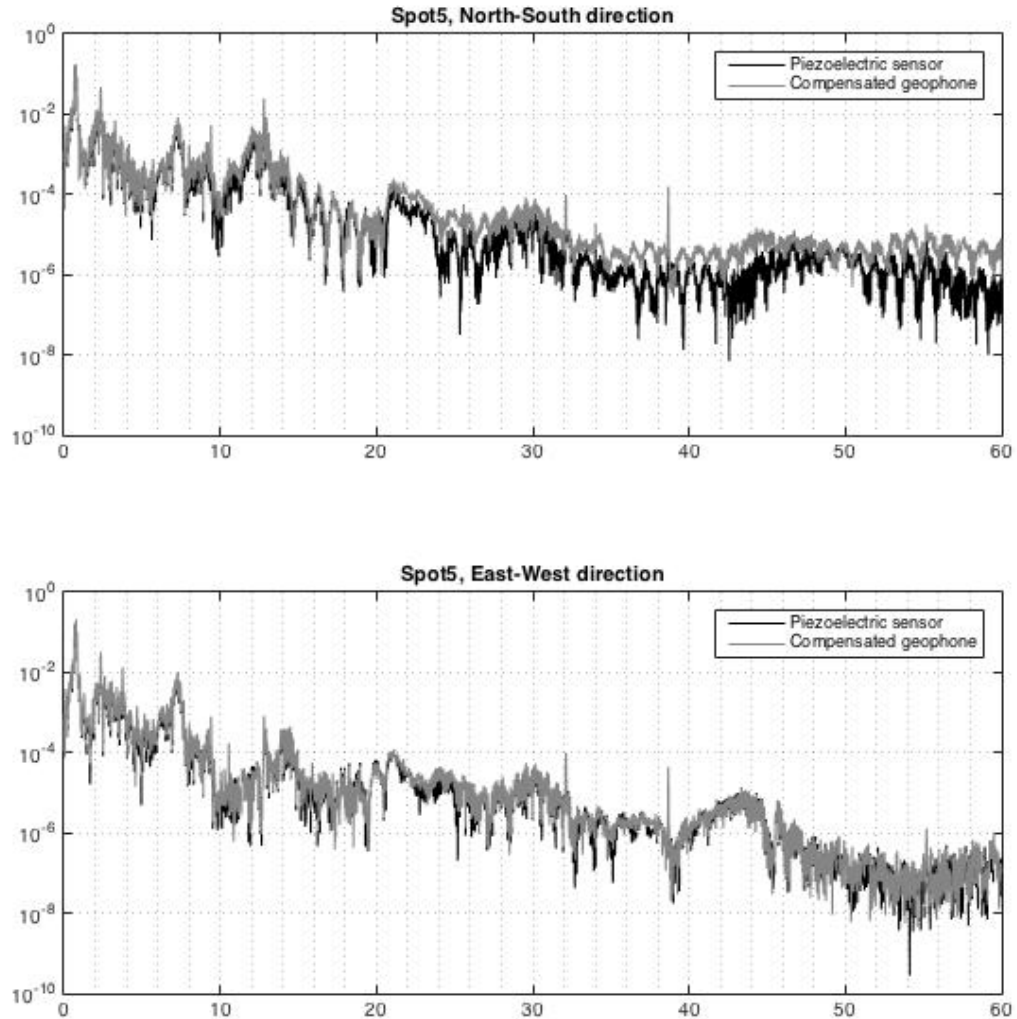


Figure 60: EV building vibration test in spot 5 (See Fig. 55)

### 6.3 Discussion of the Test Results

In the experiments that presented in previous section, we compared the compensated geophone with piezoelectric sensor. We clearly saw the differences in the results of these two sensors in laboratory condition (see Fig. 50 to Fig. 53). Due to lack of power in our portable setup, we could not sample the analog signal in our desire sample rate. Therefore, we can not see the effectiveness of the compensator in tailoring high frequency. In low frequencies, however, the geophone could capture the vibrations similar as the response of the piezoelectric sensor. This was the purpose of the compensation scheme.

# Chapter 7

## Conclusions and Future Works

### 7.1 Conclusions

Currently, use of a geophone in SHM sensing is preferable to other types of sensors due to its characteristics. The main drawback of the geophone in a sensor system is its low-frequency response. In this study, we addressed this problem to improve the geophone response in the sensor analog subsystem. We have used only passive elements in the first proposed compensator. This technique requires negative components which are only possible to have if we use active components in the circuit. After this point, we tried other techniques using active components.

For the second technique, we proposed the inverse transfer function method. A level of a lossy integrator cascaded by an integrator is responsible to cancel out the zeros in the geophone transfer function. This method appears to produce a low-pass transfer function, however, we still did not have control over the  $-3$  dB frequency of the geophone response. In order to gain this control, we moved on the next technique which is multi-loop feedback method. This method is capable of tailoring the high-frequency response of the geophone as well as improving the low-frequency response. A modified version of the multi-loop feedback method is also proposed which needs less resources to operate.

The effectiveness of the proposed circuits has been verified using a shaker in the electronic laboratory. With a shaker, we had control over the frequencies of the vibration for the sensor system. For the final evaluation, we used the modified multi-loop feedback technique in recording the vibrations of a real building and extracted the low-frequency responses of the vibrations. The benchmark to evaluate this experiments are a piezoelectric sensor that has a flat response over our frequency of interest.

### 7.2 Future Works

This study can be extended in following areas:

### **7.2.1 Analog Subsystem**

- The compensation techniques in this study are used for a specific type of geophone in SHM application. The proposed techniques can be used as the bandwidth stretching techniques for other types of analog sensors and application.
- The circuit that is used to realization of the impedance can be integrated to a chip for better performance. The chip can have adjustable gain control system for different interface and adjustable corner frequency for different geophones with different corner frequencies.

### **7.2.2 At The Sensor Level**

- The first research can be using more sensitive MEMS accelerometer instead of geophone to have smaller sensors for specific applications.
- The sensors connection to the remote device can be replaced by General Packet Radio Service (GPRS). This connection will add many different applications for the sensor. For example, the sensors can be controlled by a phone from long distance. Also for the data transmission, it will not be necessary to be in a range of a WiFi connections.

# Bibliography

- [1] GS-11D geophone specifications from Geospace Technologies inc. [Online]. Available: <http://www.geospace.com/geophones-gs-11d/>. [Accessed:15-July-2018]
- [2] PCB piezotronic product specifications. [Online]. Available: <http://www.pcb.com/Products/model/393B31>. [Accessed:23-July-2018]
- [3] GPS module specifications from ublox. [Online]. Available: <https://www.u-blox.com/en/product/max-m8q-01a-module>. [Accessed:23-July-2018]
- [4] P. Horowitz and W. Hill, *The Art of Electronics*. Cambridge University Press, 2015. [Online]. Available: <https://books.google.ca/books?id=LAiWPwAACAAJ>
- [5] S. Sah, *Encyclopaedia of Petroleum Science and Engineering*, ser. Encyclopaedia of Petroleum Science and Engineering. Kalpaz Publications, 2003, no. v. 3. [Online]. Available: <https://books.google.ca/books?id=7Pu2TMFXS8C>
- [6] R. Brincker and C. Ventura, *Introduction to Operational Modal Analysis*. Wiley, 2015. [Online]. Available: <https://books.google.ca/books?id=UQIeCgAAQBAJ>
- [7] J. Havskov and G. Alguacil, *Instrumentation in Earthquake Seismology*. Springer International Publishing, 2015. [Online]. Available: <https://books.google.ca/books?id=5PPuCgAAQBAJ>
- [8] F. Mirshafiei, M. Mirshafiei, and G. McClure, “A new three-dimensional seismic assessment method (3d-sam) for buildings based on experimental modal analysis,” *Elsevier Computers and Structures Journal*, vol. 180, pp. 125 – 137, 2017.
- [9] Tromino specifications from MOHO science and technology. [Online]. Available: <http://moho.world/en/tromino/>. [Accessed:15-July-2018]
- [10] J. Rice and B. S. G. Agha, “High sensitivity environmental sensor board and method for structural health monitoring,” Patent US 9 086 430, July 21, 2015.
- [11] A. Preumont, *Mechatronics: Dynamics of Electromechanical and Piezoelectric Systems*, ser. Solid Mechanics and Its Applications. Springer Netherlands, 2006. [Online]. Available: <https://books.google.ca/books?id=b753Dr4X0cAC>

- [12] C. Collette, P. Carmona Fernandez, S. Janssens, K. Artoos, M. Guinchard, and C. Hauviller, "Review of sensors for low frequency seismic vibration measurement," *IEEE Sensors Journal*, vol. 3, no. 2, pp. 36–41, Jan 2011.
- [13] C. Collette, L. Fueyo-Roza, and M. Horodincea, "Prototype of a small low noise absolute displacement sensor," *IEEE Sensors Journal*, vol. 14, no. 1, pp. 91–95, Jan 2014.
- [14] R. Brincker, T. L. Lagö, P. Andersen, and C. Ventura, "Improving the classical geophone sensor element by digital correction," *IEEE Sensors Journal*, pp. 56–61, Jan 2005.
- [15] Y. Zhang, Z. Zou, and H.-w. Zhou, "Estimating and recovering the low-frequency signals in geophone data," *Journal of SEG (Society of Exploration in Geophysics)*, pp. 1–5, Sep 2012.
- [16] K. Song, Y. Yang, Y. Guo, S. Tong, and L. Dong, "A low-frequency geophone designed by genetic algorithms," in *2017 IEEE International Geoscience and Remote Sensing Symposium (IGARSS). Texas, USA*, July 2017, pp. 3421–3424.
- [17] W. R. Mitchell, "Short period seismic system with long period response," Patent US 3 412 374, 11 19, 1968.
- [18] J. Hosken, "Some electronic simulators of galvanometers and geophones, and their use for inverse filtering," *Journal of Geophysical Prospecting*, vol. 13, no. 3, pp. 362–386. [Online]. Available: <https://onlinelibrary.wiley.com/doi/abs/10.1111/j.1365-2478.1965.tb01939.x>
- [19] Low noise, low drift, low power, 3-axis MEMS accelerometers from Analog Devices Inc. [Online]. Available: [http://www.analog.com/media/en/technical-documentation/data-sheets/ADXL354\\_355.pdf](http://www.analog.com/media/en/technical-documentation/data-sheets/ADXL354_355.pdf). [Accessed:15-July-2018]
- [20] N. Hakimitoroghi, A. Sabamehr, R. Raut, M. Mirshafiei, and A. Bagchi, "Comparative study on two types of sensors for measuring vibration response of building structures," in *The 8th International Conference on Structural Health Monitoring of Intelligent Infrastructure (SHMII), Sydney, Australia*, Dec 2017, pp. 1–5.
- [21] M. Guan and W.-H. Liao, "Studies on the circuit models of piezoelectric ceramics," in *International Conference on Information Acquisition 2004, Proceeding. Hefei, China*, June 2004, pp. 26–31.
- [22] M. Abrams and A. Keith Elder, "Dynamic range in a seismic channel," *First Break Journal*, vol. 31, pp. 79–87, Jan 2013.
- [23] STM32L4 microcontroller manufacturer website. [Online]. Available: <https://www.st.com/en/microcontrollers/stm32l4-plus-series.html?querycriteria=productId=SS2002>. [Accessed:15-July-2018]
- [24] 32-bit oversampling adc with configurable digital filter from Analog Devices Inc. [Online]. Available: <http://www.analog.com/media/en/technical-documentation/data-sheets/250832fc.pdf>. [Accessed:15-July-2018]

- [25] DSUT network information provided by Analog Devices. [Online]. Available: <http://www.analog.com/en/applications/technology/smartmesh-pavilion-home.html>. [Accessed:15-July-2018]
- [26] P. W. Rodgers, "Maximizing the signal-to-noise ratio of the electromagnetic seismometer: The optimum coil resistance, amplifier characteristics, and circuit," *Bulletin of the Seismological Society of America*, vol. 2, pp. 561–582, 1993.
- [27] R. Raut and M. Swamy, *Modern Analog Filter Analysis and Design: A Practical Approach*. John Wiley & Sons, 2010. [Online]. Available: <https://books.google.ca/books?id=n4KglfxUhoQC>
- [28] Piezoelectric driver circuit from PCB PIEZOELECTRONICS. [Online]. Available: [http://www.pcb.com/Resources/Technical-Information/tipsfromtechs/Powering\\_ICP\\_Accelerometers](http://www.pcb.com/Resources/Technical-Information/tipsfromtechs/Powering_ICP_Accelerometers). [Accessed:15-July-2018]
- [29] LTC2508-32 demo board — 32-bit over-sampling ADC with configurable digital filter. [Online]. Available: <http://www.analog.com/en/design-center/evaluation-hardware-and-software/evaluation-boards-kits/dc2222a-b.html>. [Accessed:15-July-2018]